The prolyl isomerase FKBP25 regulates microtubule polymerization impacting cell cycle progression and genomic stability

David Dilworth[1], Geoff Gudavicius[1], Xiaoxue Xu[2], Andrew K.J. Boyce[2], Connor O'Sullivan[1], Jason J. Serpa[3], Misha Bilenky[4], Evgeniy V. Petrochenko[3], Christoph H. Borchers[3], Martin Hirst[4], Leigh Anne Swayne[2,5], Perry Howard[1] and Christopher J. Nelson[1,*]

[1]Department of Biochemistry and Microbiology, University of Victoria, Victoria, BC, V8W 3P6, Canada, [2]Division of Medical Sciences and Island Medical Program, University of Victoria, Victoria V8P 5C2, Canada, [3]University of Victoria Genome BC Proteomics Centre, Vancouver Island Technology Park, Victoria, BC, V8Z 7X8, Canada, [4]BC Cancer Agency Genome Sciences Centre and the Department of Microbiology & Immunology, Michael Smith Laboratories, University of British Columbia, Vancouver, BC, V6T 1Z3, Canada and [5]Department of Cellular and Physiological Sciences, University of British Columbia, Vancouver V6T 1Z3, Canada

ABSTRACT

FK506 binding proteins (FKBPs) catalyze the interconversion of *cis-trans* proline conformers in proteins. Importantly, FK506 drugs have anti-cancer and neuroprotective properties, but the effectors and mechanisms underpinning these properties are not well understood because the cellular function(s) of most FKBP proteins are unclear. FKBP25 is a nuclear prolyl isomerase that interacts directly with nucleic acids and is associated with several DNA/RNA binding proteins. Here, we show the catalytic FKBP domain binds microtubules (MTs) directly to promote their polymerization and stabilize the MT network. Furthermore, FKBP25 associates with the mitotic spindle and regulates entry into mitosis. This interaction is important for mitotic spindle dynamics, as we observe increased chromosome instability in FKBP25 knockdown cells. Finally, we provide evidence that FKBP25 association with chromatin is cell-cycle regulated by Protein Kinase C phosphorylation. This disrupts FKBP25–DNA contacts during mitosis while maintaining its interaction with the spindle apparatus. Collectively, these data support a model where FKBP25 association with chromatin and MTs is carefully choreographed to ensure faithful genome duplication. Additionally, they highlight that FKBP25 is a MT-associated FK506 receptor and potential therapeutic target in MT-associated diseases.

INTRODUCTION

In proteins, proline is found in both the *cis* and *trans* peptide bond conformation. Since ∼5% of prolines in folded proteins adopt the *cis* conformation, the dynamic interconversion of proline isomers may represent a fundamental property of most proteins (1,2). Peptidyl-prolyl isomerase (PPI) enzymes regulate the isomerization rate of prolines. Three evolutionarily conserved and structurally distinct families classify PPIs: the parvulins, cyclophilins (Cyps) and FK506 binding proteins (FKBPs) (3). The latter two are together referred to as immunophilins because of their association with the immunosuppressant drugs cyclosporin and FK506/rapamycin.

Based on subcellular localization and protein interaction data, PPIs participate in a variety of processes from the cell surface to the nucleolus (4–12). Most, but not all, PPIs have additional domains thought to aid recruitment of their prolyl isomerase activities to client proteins. However, an important and emerging theme in the study of immunophilins is that some FKBP and Cyp domains have functions separate from their ascribed prolyl isomerase activity. Essentially, these enzymes can regulate protein function via binding and/or catalytic events.

Several prolyl isomerases are implicated in the regulation of microtubules (MTs) and associated protein folding pathologies. For instance, the microtubule-associated protein (MAP) tau aggregates into paired neurofibrillary tangles, which reduces its capacity to stabilize MTs. Tau aggregates are a pathological hallmark of Alzheimer's disease and related neurodegenerative disorders, coined tauopathies (13). Strikingly, the *cis-trans* conformational state of a single proline residue in tau is indicative of either the pathogenic or

---

*To whom correspondence should be addressed. Tel: +1 250 853 3889; Email: cjn@uvic.ca

biologically active state (14). Pin1, a member of the parvulin PPI family, FKBPs and Cyps are each reported to regulate Tau folding (14–16), which underscores the importance of PPI regulation of Tau function.

PPIs can regulate MT dynamics independently of their catalytic activity. For instance, the PPI FKBP52 destabilizes MTs through direct binding of tubulin and not through prolyl-isomerization (17). Several of the hsp90-associated immunophilins are also known to interact with the MT network, including: CypA (18), Cyp40 (19), FKBP52 (18,20), FKBP51 (20), FKBPL (21) and FKBP15 (22). Interestingly, the immunomodulatory drug FK506, which targets the catalytic pocket of FKBPs, has been shown to have neuroprotective and regenerative qualities (23), leading to the term 'neuroimmunophilin' to describe the FKBP effectors in neurons that mediate this response. Collectively these reports establish that many immunophilins occupy the dynamic MT network and that both catalytic and binding mechanisms appear to be involved in PPI regulation of MTs.

FKBP25 is a nucleic acid binding immunophilin that shuttles between the nucleus and cytoplasm, and associates with chromatin modifying enzymes (24–28). Because of these features it has been proposed that FKBP25 functions as a transcriptional regulator. FKBP25 contains a structurally unique N-terminal Basic Tilted Helical Bundle domain (BTHB) (29), tethered by a 54-amino acid flexible linker region to a C-terminal conserved FKBP PPI domain. Studies to date have drawn connections between FKBP25 and the regulation of ribosome biogenesis (30,31), chromatin (28) and the tumor suppressor p53 (27). However, there is limited direct evidence to support any conclusions with respect to how FKBP25 influences DNA- or RNA-centric processes. Here, we confirm that FKBP25 binds nucleic acids but is also a MAP. The catalytic FKBP domain of FKBP25, but not its catalytic prolyl isomerase action, stabilizes the MT network via direct binding to MTs, which promotes their polymerization. Consistent with a critical role in MT function, FKBP25 is required for cell cycle progression and faithful chromosome segregation. Finally, we provide insight into how this FKBP is regulated: we demonstrate that FKBP25 is phosphorylated during mitosis by Protein Kinase C (PKC) at a key DNA binding interface. This phosphorylation event displaces FKBP25 from chromatin to promote its localization to the mitotic spindle. Our results demonstrate that FKBP25 is a novel MAP that engages both nucleic acids and MTs, and that these interactions are controlled by carefully timed phosphorylation events to ensure proper cell division and genome segregation.

MATERIALS AND METHODS

Cell culture, transfections and generation of stable cell lines

U2OS (ATCC), Flp-In T-Rex HEK293 (Thermo Fisher), Flp-In T-Rex U2OS (a generous gift from Dr Blerta Xhemalce, University of Texas at Austin) and Flp-In HeLa S3 (graciously provided by Dr Till Bartke, Imperial College London) cells were cultured in Dulbecco's modified Eagle's medium containing 10% (v/v) Fetal Bovine Serum (Sigma, St Louis, MO, USA) and antibiotics (10 units/ml penicillin and 10 μg/ml streptomycin, ThermoFisher, Waltham,

MA, USA) at 37°C and 5% CO_2. For transient siRNA knockdown, reverse transfection of 10 nM targeting or non-targeting control siRNA was performed using jetPRIME (Polyplus-transfection, Illkirch-Graffenstaden, France) following the manufacturer's instruction, followed by incubation for 48–72 h before downstream analysis. Stable U2OS shRNA knockdown cells were generated by transfection with HuSH 29-mer shRNA expression vectors (Origene, Rockville, MD, USA) using GenJet U2OS Transfection Reagent (SignaGen, Rockville, MD, USA) followed by selection with puromycin (InvivoGen, San Diego, CA, USA) 48 h post-transfection until colonies formed. Colonies were then isolated, expanded and screened for knockdown by western blot and reverse transcriptase-quantitative polymerase chain reaction (RT-qPCR).

RNAi targeting sequences

siRNA/shRNA	Sequence	Manufacturer
siCNTRL	5′-AAGATCATACGTGCGAT CAGA-3′	Eurofins Genomics
siGFP	5′-AAGGCTACGTCCAGGAG CGCACC-3′	Eurofins Genomics
siFKBP25	5′-AACCACTTGGTTACAGC CTAT-3′	Eurofins Genomics
shCNTRL	5′-CACAAGCTGGAGTACAA CTACAACAGCCA-3′	OriGene (TR30001)
shFKBP25.1	5′-CAGGAACACGGTTCAGA TTCGTTTCTTGC-3′	OriGene (TR319727B)
shFKBP25.2	5′-TCGGAGTAGGCAAAGTT ATCAGAGGATG-3′	OriGene (TR319727D)

Plasmids

Plasmids containing expression vectors for stable integration and tetracycline-inducible expression were generated by subcloning a synthesized FKBP25–3xFLAG-6xHIS gene (GenScript, Piscataway, NJ, USA) into a modified pcDNA5/FRT/TO vector (Thermo Fisher). For plasmids used to generate Flp-In T-Rex U2OS T-Rex lines used in siRNA rescue experiments, a stop codon was introduced before the 3xFLAG-6HIS tag to generate a tagless FKBP25 construct as well as silent mutations in the siRNA targeting sequence by site-directed mutagenesis. His-tag bacterial expression vectors were generated by cloning synthesized FKBP25 genes (GenScript) into a pET 6-His vector using standard techniques. Site-directed mutagenesis of pcDNA5 and pET 6-His vectors was accomplished by inverse PCR with mutagenic primers. All constructs were validated by sequencing.

Recombinant proteins

FKBP25 6-His proteins were expressed in *Escherichia coli* BL21 (DE3) cells grown overnight, diluted 1:20 and induced at an OD600 of 0.6 with 1 mM Isopropyl β-D-1-thiogalactopyranoside (IPTG) for 4 h. Cell pellets were resuspended in binding buffer (50 mM Tris pH 8, 150 mM NaCl, 0.5% NP-40, 5 mM ethylenediaminetetraacetic acid (EDTA), 1 μg/ml leupeptin, 1 μg/ml aprotinin and 1 μg/ml pepstatin), sonicated and cleared by centrifugation. Recombinant 6-His proteins from cleared lysates were

purified using Nickel-NTA agarose (Qiagen, Hilden, Germany) following the manufacturer's protocol and dialyzed overnight in $1\times$ phosphate-buffered saline (PBS) containing 10% glycerol. Histone H3 was expressed in *E. coli* BL21 (DE3) and purified to homogeneity through acid extraction, ion exchange (Macro-Prep Ion Exchange Media, BioRad, Hercules, CA, USA) and reverse phase HPLC (C18–300, 250 mM $\times$ 4.5 mM, 5 μM, ACE). Histone H1 was sourced from Roche (Basel, Switzerland). PKCα and PKCβII kinases purchased from SignalChem (Richmond, Canada). CDK1-cyclinB1 and CKII kinases were purchased from New England Biolabs (Ipswich, MA, USA).

Antibodies

The following antibodies were used in this study: GAPDH (Santa Cruz, Santa Cruz, CA, USA; sc-47724-WB 1:10 000), FKBP25 (GenScript: WB 1:2000; IF 1:300), α-Tubulin (Santa Cruz; sc8035-WB 1:10 000, IF 1:1000), H3pS10 (Abcam, Cambridge, UK; ab5176-WB 1:10 000 flow cytometry 1:5000), Annexin V (Santa Cruz; sc-4252 FITC-flow cytometry 1:300), Histone H3 (Abcam; ab1791-WB 1:50 000), Parp-1 (Santa Cruz; sc-8007-WB 1:5000) and p53 (Santa Cruz; sc126-WB 1:5000).

Phos-tag SDS-PAGE, and western blotting

Western blots were performed by resolving proteins by sodium dodecyl sulphate-polyacrylamide gel electrophoresis (SDS-PAGE) and transferring to nitrocellulose membranes in phosphate transfer buffer (50 mM sodium phosphate buffer pH 6.8, 15% EtOH). For Phos-tag western blots, SDS-PAGE gels included 50 μM Phos-tag (Wacko Pure Chemicals Industry Ltd, Madrid, Spain) and 10 mM MnCl$_2$. Phos-tag-SDS-PAGE gels were washed twice in a solution of transfer buffer containing 100 mM EDTA before transfer, as previously described (32). Membranes were incubated in 10% skim milk for 30 min to block and probed with primary antibody for either 1 h at room temperature or overnight at 4°C followed by three washes in TBS-T (1$\times$ TBS with 0.1% Tween 20). For chemiluminescence-based detection, horseradish peroxidase conjugated anti-mouse (GE, Boston, MA, USA) or anti-rabbit (GE) secondary antibody was used at 1:5000 in 1% milk/TBS-T. Blots were then washed three times in TBS-T and proteins detected by incubation with a chemiluminescence HRP substrate (Millipore, Billerica, MA, USA) and exposed to film. For fluorescence-based detection, blots were incubated with either IRdye 800CW anti-mouse (Mandel Scientific, Guelph, Canada) or IRdye 680RD anti-rabbit (Mandel Scientific) at 1:5000 for 1 h at room temperature in 1% milk TBS-T, followed by three washes in TBS-T and one wash in 1$\times$ TBS, and imaging on an Odyssey Clx imaging system (Li-Cor, Lincoln, Nebraska).

MTT proliferation assay

Assays were performed as previously described (33). Briefly, cells reverse transfected with siRNA were incubated overnight, then trypsinized, counted by hemocytometer and plated at densities ranging from 5000 to 15 000 cells per well of a 96-well plate. Plates were incubated for 72 h, and 20 μl of 5 mg/ml thiazolyl blue tetrazolium (Sigma) was added to each well and incubated for 2.5–3 h at 37°C. Media was removed and 150 μl of dimethyl sulfoxide (DMSO) added per well to solubilize the precipitant. Plates were incubated for a further 15 min at room temperature with shaking and samples were read at OD 595nm and OD 630 nm, as a reference, on an absorbance microplate reader (BioTek, Winooski, Vermont).

Cell cycle analysis

Cells were harvested by trypsinization and centrifugation at 300 $\times$ g for ten minutes at 4°C. Cell numbers were determined by counting with a hemocytometer and 1×10^6 cells per sample were aliquoted in tubes, washed in 1 ml $1 \times$ PBS, and resuspended in 300 μl $1 \times$ PBS. Cells were then fixed with 700 μl of 100% ice cold ethanol added dropwise with gentle vortexing to a final concentration of 70% and incubated overnight at -20°C. For experiments where cells were co-stained for the mitotic marker H3pS10 and propidium iodide, fixed cells were resuspended in 1 ml of 0.25% Triton in $1 \times$ PBS (PBS-T) and incubated for 10 min on ice to permeabilize the membrane. Permeabilized cells were pelleted as above and incubated in 500 μl of $1 \times$ PBS containing 1% bovine serum albumin (BSA) to block non-specific binding. A polyclonal antibody for H3pS10 (Abcam, ab5176) was diluted 1:5000 in PBS-T and 150 μl was added to each sample and incubated for 1–1.5 h at room temperature. Cells were then washed one time in 1 ml of $1 \times$ PBS and resuspended in 150 μl of goat anti-rabbit AlexaFluor 488-conjugated antibody (ThermoFisher) diluted 1:300 in PBS-T. Samples were incubated for 1 h in secondary antibody at room temperature before continuing with the protocol for PI staining. To stain DNA with PI, cells were washed once with $1 \times$ PBS and then resuspended in 0.25 ml $1 \times$ PBS with 0.5 mg/ml RNase A (Qiagen) and incubated for 1 h at 37°C. Following RNase A treatment 10 μl of 1 mg/ml PI (Sigma) was added to each sample and incubated for 30 min in the dark at room temperature. Fixed and stained cells were washed, filtered, and analyzed by flow cytometry on a BD FacsCalibur (BD Biosciences, Franklin Lakes, NJ, USA).

Cell synchronization

Synchronization of cells was accomplished by treating cells with reversible cell cycle arresting agents, followed by two washes with warmed 1x and release into fresh media. Double thymidine blocks were used to arrest cells at early S phase, by treating cells with 2 mM thymidine (Sigma) for 18 h followed by release for 9 h and treatment with 2 mM thymidine for an additional 17 h before release into S phase. To arrest cells in M-phase, cells were first arrested at early S by a 24 h thymidine block as above followed by treatment with 100 ng/ml nocodazole (Sigma) for 12 h. To release from nocodazole cells were harvested by mitotic shake off, washed with $1 \times$ PBS and reseeded in fresh media. Synchronization of cells at G2/M was accomplished by first blocking cells in early S phase by 24 h treatment with 2 mM thymidine followed by 12 h treatment with 9 μM RO-3306 (Santa Cruz), a potent CDK1 inhibitor. Cells were then released

into mitosis by two washes with 1 × PBS and supplemented with fresh media.

Immunoprecipitation

HeLa S3 cells stably expressing an FKBP25–3xFLAG transgene or a parental control were synchronized in various stages of the cell cycle as described, harvested by cell scraper, and pelleted by centrifugation at 300 × g in a swinging bucket rotor. Whole cell extracts were prepared by resuspending cell pellets directly in Immunoprecipitation (IP) wash buffer with protease and phosphatase inhibitors (50 mM Tris pH8, 150 mM NaCl, 0.5% NP-40, 0.5% Triton X-100, 2 mM EDTA, 1 μg/ml aprotinin, 1 μg/ml leupeptin, 1 μg/ml pepstatin, 5 mM β-glycerophosphate, 10 mM NaF, 20 mM $Na_4P_2O_7$, and 2 mM Na_3VO_4) and sonicated on high for 5 min with 20 s ON/OFF cycles on ice. Insoluble material was pelleted by centrifugation at 12 000 × g for 15 min and normalized by Bradford assay. Whole cell extracts were added to pre-washed EZ-view Red ANTIFLAG M2 Affinity gel beads and incubated at 4°C for 1.5–3 h with nutating. After binding, beads were washed three times with IP wash buffer. Bound FLAG-tagged FKBP25 from synchronized cells was eluted by competition with 3xFLAG peptide (Sigma), by beads in 150 ng/μl peptide in 1 × TBS for 20 min at 4°C. Eluted material was run on SDS-PAGE gels with or without 50 μM Phos-tag and transferred by blotting or further processed for mass spectrometry analysis of phosphorylated residues.

Immunofluorescence

For imaging of interphase and mitotic cells, U2OS cells were seeded on 8-well glass slides (Millipore) and either synchronized at the G2/M transition and released as described or grown asynchronously. Immunofluorescence staining was performed by first washing cells once with 1 × PBS and fixing with a 3.7% Paraformaldehyde (PFA) in PBS solution for 10 min at room temperature. Fixed cells were permeabilized for 10 min on ice using 0.5% Triton X-100 in 1 × PBS and then blocked for 30 min in PBS-T (0.1% Tween 20 in PBS) containing 1% BSA at room temperature. Slides were then incubated with primary antibody diluted in PBS-T for 1 h at room temperature followed by three 5 min washes in PBS. After washing, the slides were then incubated with secondary antibodies, AlexaFluor 488 goat anti-mouse (Life Technologies) and goat anti-rabbit IgG-CFL 555 (Santa Cruz), in PBS-T for 1 h and washed three times with 1 × PBS. Coverslips were mounted using Fluoroshield with DAPI (Sigma) and sealed with clear nail polish. Slides were then imaged on an SP8 confocal microscope (Leica, Wetzlar, Germany) or a DM IRE2 epi-fluorescence microscope (Leica) and images processed using the Fiji distribution of ImageJ (34).

Microtubule purification and spin-down binding experiments

MTs and MAPs were purified for binding experiments as previously described (35,36). Harvested asynchronous or thymidine-nocodazole arrested HeLa cells were weighed and homogenized in 1 ml of PME Buffer with detergent containing protease and phosphatase inhibitors (100 mM Pipes pH 6.9, 1 mM $MgCl_2$, 2 mM ethylene glycol-bis(β-aminoethyl ether)-N,N,N',N'-tetraacetic acid (EGTA), 1 mM Dithiothreitol (DTT), 0.5% NP-40, 1 μg/ml aprotinin, 1 μg/ml leupeptin, 1 μg/ml pepstatin, 5 mM β-glycerophosphate, 10 mM NaF, 20 mM Na_4P2O_7, and 2 mM 2 mM Na_3VO_4) per gram of cells. The homogenate was then centrifuged at 100 000 × g for 60 min at 4°C in a TLA-100.3 rotor (Beckman, Brea, CA, USA). Cleared supernatant was incubated at 37°C for 15–20 min with 20 μM paclitaxel (Sigma) and 0.1 mM GTP (Sigma). The sample was then underlain with PME containing 10% sucrose and 10 μM paclitaxel and centrifuged at 45 000 × g for 30 min at 25°C in a TLA-100.3 rotor (Beckman). Following pelleting of MTs, the supernatant was removed and the tube gently rinsed with room temperature PME buffer. The pellet was resuspended in PME buffer containing 10 μM paclitaxel and centrifuged over a second PME sucrose cushion as above before being resuspended in PME buffer and flash frozen. For MT spin-down binding experiments 5 μg of recombinant FKBP25 was added to 25 μg of purified MTs and incubated at 37°C for 30 min to allow binding to occur. The mixture was overlaid on a sucrose cushion as described and centrifuged at 45 000 × g for 30 min at 25°C in a TLA-100.3 rotor. The supernatant (unbound fraction) was removed, and Laemmeli sample buffer added. The pellet (bound fraction) was washed one time in warm PME buffer before being resuspended in Laemmeli sample buffer. Samples were resolved by SDS-PAGE and western blotting.

Microtubule polymerization assays

MT polymerization assays were performed using a fluorescence-based Tubulin Polymerization kit (Cytoskeleton Inc, Denver CO, Cat. # BK011P) following the manufacturer's instructions.

Mass spectrometry analysis of phosphorylated proteins

To identify phosphorylated sites on FKBP25 purified FLAG-tagged FKBP25 from mitotic HeLa S3 cells or *in vitro* phosphorylated recombinant FKBP25, samples were first digested overnight with either AspN or trypsin at 37°C and lyophilized until dry. Peptides were resuspended in water and desalted/purified by passing through C18 ZipTips (Millipore). Samples were then analyzed on an Orbitrap LTQ mass spectrometer and phosphorylated peptides identified using the MASCOT server (Matrix Science, Boston, MA, USA).

In cell microtubule stability assays

In cell MT stability assays were performed as described previously (37). For blotting analysis of shRNA stable knockdown cells, cells were first harvested by trypsinization, washed twice in PME buffer and then incubated with PME buffer (100 mM Pipes pH 6.9, 1 mM $MgCl_2$, 2 mM EGTA) supplemented with 0.05% Triton X-100 (w/v) and protease inhibitors (1 μg/ml aprotinin, 1 μg/ml leupeptin and 1 μg/ml pepstatin) at 37°C for 30 min. Samples were then centrifuged at 15 000 × g for 30 min and the supernatant (S

fraction) containing solubilized tubulin was removed and the pellet (P fraction) containing sedimented polymerized tubulin was washed once in PME buffer. Laemmli sample buffer was added to both samples to 1× at equal volumes and the samples were resolved by SDS-PAGE and western blotting. For knockdown/rescue immunofluorescence experiments, U2OS-T-Rex-Flp-In cells harboring siRNA-resistant tagless FKBP25 transgenes (wild-type sequence or Y198F mutant) were cultured in the absence or presence of 0.1 μg/ml tetracycline (Sigma) for 24 h to induce expression of the rescue allele, transfected with 10 nM siRNA overnight as described, then seeded on 8-well glass slides (Millipore) in media with (transgene rescue) or without 0.1 μg/ml tetracycline (Sigma) and cultured for an additional 48 h. Cells were washed once with 1× PBS then incubated with PME buffer with protease inhibitors and 0.5% Triton X-100 for 5 min at room temperature and washed one time in 1× PBS before immunofluorescence staining and imaging as described.

Quantification of micronuclei and binucleated cells

To quantify the frequency of micronucleated cells, U2OS stably expressing FKBP25 targeting or control shRNA were seeded in 8-well glass slides (Millipore) and incubated overnight. The following day cells were washed 1 × with PBS and fixed with 3.7% PFA. Cells were mounted in FluroShield mounting media containing DAPI (Sigma) and slides sealed with nail polish. For each stable cell line at least five fields of view were imaged with a Leica DM IRE2 epi-florescent microscope. The number of micronuclei (MN) and intact nuclei was counted per image using ImageJ software. For the quantification of bi-nucleated cells, shRNA stable cells were seeded in 12-well plates at a low density to avoid clumping and reduce ambiguity between bi-nucleated and adjacent or overlapping cells. The following day cells were fixed in methanol for 5 min at room temperature and allowed to air dry. Next plates were stained with 1:20 diluted Giemsa stain (Sigma) for 1 h at room temperature and rinsed with deionized water. Plates were allowed to air dry prior to imaging on a Leica DM IRE2 microscope and counting with ImageJ software. For both experiments, all image file names were randomized prior to quantification.

Crystal violet staining

Stable U20S cell lines expressing the shRNAs to GFP or FKBP25 were seeded in 24-well plates. When cells reached 40–50% confluence they were treated with the indicated paclitaxel concentrations for 24 h, recovered in paclitaxel-free media for 24 h and subjected to crystal violet staining.

In vitro kinase assays

For kinase assays using HEK293 cell extracts, extracts were prepared as previously described (38,39). Thymidine/nocodazole-synchronized mitotic cells were harvested by mitotic shake off and resuspended and washed twice in EBS buffer containing protease inhibitors (40 mM β-glycerophosphate pH 7.3, 15 mM MgCl₂, 20 mM EGTA, 2 mM adenosine triphosphate (ATP), 1 mM glutathione, 1 μg/ml aprotinin, 1 μg/ml leupeptin and 1 μ/ml pepstatin), and flash frozen in liquid nitrogen. After thawing, the suspension was passed through a 27 G needle 10 times, followed by ultracentrifugation (∼54 000 × G for 10 min in a TLA100.3 rotor [Beckman]). The supernatant was again centrifuged at ∼54 000 × G, removed and supplemented with 250 mM sucrose. The protein concentration of extracts was measured by Bradford assay, adjusted to 15 mg/ml and aliquots were flash frozen in liquid nitrogen and stored at −80°C. For *in vitro* phosphorylation with mitotic extract 3 μg of protein was incubated with 2 μl of extract in EBS buffer supplemented with 1 μCi γ[^{32}P] ATP. Reactions were incubated for 30 min at 30°C and one-fourth of each reaction was resolved by SDS-PAGE. Gels were dried, exposed to a phosphor screen (Molecular Dynamics), and imaged on a Phosphorimager (STORM, GE Healthcare). For *in vitro* phosphorylation reactions with commercial recombinant kinases, 1 μg of recombinant protein was incubated with kinases following the manufacturer's recommendations and incubated for 30 min at 30°C.

Gel retardation assay

Plasmid-based *in vitro* DNA binding assay was performed as previously described (28). Increasing amounts of FKBP25 were mixed at DNA: FKBP25 molar ratios of 1:0, 1:25, 1:50, 1:100. The mixture was incubated for 30 min at room temperature and loaded on a 1% agarose gel. Gels were visualized by ethidium bromide staining on an AlphaImager (ProteinSimple, San Jose, CA, USA).

Annexin V apoptosis assay

To measure induction of apoptosis cells were treated with 50 mM etoposide (Sigma) for 24 h and processed using the Annexin V Apoptosis Kit from Santa Cruz (sc-4252 AK) following the manufacturer's protocol. Briefly, cells were trypsinized for 5 min at 37°C and collected in 15 ml falcon tubes. To pellet, cells were spun at 300 × g for 5 min and washed twice in ice-cold 1 × PBS then resuspended in 1 × Assay Buffer at a concentration of 1 × 10⁶ cells/ml. To each 1 μl of Annexin V FITC and 10 μl of PI was added per 100 μl of cells. Cells were then gently vortexed and incubated for 15 min at room temperature in the dark. A total of 400 μl of Assay Buffer was added to each sample, which was then analyzed by flow cytometry on a BD FacsCalibur.

Clonogenic survival assay

For clonogenic survival assays, performed as previously described (40), cells were plated at low density in 6-well plates (500–1500 cells/well) and incubated overnight. The following day, cells were treated for 1 h with etoposide (Sigma), camptothecin (Sigma) or X-ray irradiated at the BC Cancer Agency, Royal Jubilee Hospital. Plates were incubated for ∼14 days until colonies of sufficient size were formed, changing media every 3–4 days. For fixation, media was removed and cells washed in 1 × PBS and 2 ml of fixative solution (acetic acid: methanol 1:7) was added and left for 5 min at room temperature. Fixation solution was removed and 1

ml of 0.5% crystal violet was added per well and incubated for 2 h at room temperature. The crystal violet solution was removed by rinsing plates in tap water and the plates were allowed to air dry overnight. Plates were then imaged on a flatbed scanner and analyzed using the ColonyArea plugin for ImageJ (41).

RNA-Seq, gene ontology and network analysis

siRNA treated HEK293 samples were processed and sequenced at the BC Cancer Agency Michael Smith Genome Sciences Centre following standard operating protocols. Briefly, oligo(dT) purification of mRNA was performed using the μMACs mRNA isolation kit (Miltenyl Biotec, Bergisch Gladbach, Germany) and analyzed on an Agilent 2100 Bioanalyzer using Agilent 6000 RNA Nano Kit (Agilent Technologies, Santa Clara, CA, USA). cDNA was generated using the Superscript Double-Stranded cDNA Synthesis kit (ThermoFisher), 75 bp paired-end libraries prepared using the Paired-End Sample Prep Kit (Illumina, San Diego, CA, USA) and sequenced on a HiSeq 2000 sequencing system (Illumina). Paired-end reads were aligned to the UCSC hg19 human reference genome using the HISAT2 alignment program (42). Ranked lists of differentially expressed genes were generated using GFOLD (43). For KEGG pathway analysis, ranked lists with a log fold change either >0.5 or <0.5 were submitted to the DAVID (Database for Annotation, Visualization and Integrated Discovery version 6.8) web server (44). Network analysis of RNA-Seq data was carried out using the R package clusterProfiler (45). RNA-seq data have been deposited with the following accession code: GSE100813

RESULTS

Disruption of FKBP25 attenuates G1/S and G2/M transitions of the cell cycle

FKBP25 localizes to the nucleus, directly binds nucleic acids and associates with chromatin modifying enzymes (26,28,30). However, the implications of these features on transcription have not been addressed. To answer this question, we performed RNA sequencing to compare transcriptomes from HEK293 cells transfected with either FKBP25 targeting siRNA or a GFP targeting control siRNA (Figure 1). Surprisingly, changes in overall gene expression were subtle; suggesting FKBP25's role in transcriptional regulation is minimal in this cell line. When we explored Kyoto Encyclopedia of Genes and Genomes (KEGG) pathway enrichment of ranked differential expression, we found enrichment in signaling factors involved in cell cycle regulation, including activation of mitogen-activated kinase (MAPK) stress response signaling and decreased expression of genes associated with metabolic processes (Figure 1B–E and Supplementary Figure S1). In agreement with this altered expression profile, there was a significant decrease in cellular proliferation when FKBP25 was disrupted (Supplementary Figure S2), indicating that FKBP25's function within the cell contributes to cell cycle progression.

To explore the role for FKBP25 in cell cycle regulation, we performed siRNA knockdowns in U2OS cells and quantified proliferation by the MTT assay, noting a significant

decrease when FKBP25 was depleted (Figure 2A and B). To measure changes in the cell cycle, cells were stained with the mitotic marker H3pS10 and propidium iodide (PI) 72 h post-transfection (Figure 2C–E). FKBP25 depleted cells displayed decreased S-phase content, increased G0/G1 and G2 populations and fewer cells actively undergoing mitosis. To further dissect FKBP25 regulation of the cell cycle we measured cell cycle distributions after an 8 h nocodazole block, which halts progression in mitosis (Figure 2F). We found that depletion of FKBP25 reduced entry into S-phase and mitosis (Figure 2G–I), suggesting that FKBP25 plays a role in G1/S and G2/M transitions. This phenotype was confirmed using stable cell lines expressing independent shRNAs targeting FKBP25 (Figure 2J). Nocodazole trap and H3pS10 western blotting again showed impaired entry into mitosis when we target FKBP25 expression. Interestingly, the tumor suppressor p53 has been demonstrated to downregulate transcription of FKBP25 (46), suggesting halting of the cell cycle by p53, which enforces both G1/S and G2/M checkpoints (47), may in part be facilitated by FKBP25. While FKBP25 has also been shown to directly stimulate auto-ubiquitylation of MDM2 resulting in stabilization of p53 (27), we did not see a significant reduction in p53 levels with depletion of FKBP25 (Supplementary Figure S3), thus this may be a cell type-specific phenomenon.

To determine if FKBP25 specifically influences entry into mitosis, cells were synchronized at the G2/M boundary by thymidine block followed by treatment with RO-3306, a potent and selective inhibitor of CDK1 (48), and released (Figure 2K). Cells depleted of FKBP25 by siRNA exhibited a delay in the entry into mitosis (Figure 2L). Similarly, PI-staining of stable shRNA knockdown cells confirmed delayed progression through mitosis and into G1 (Figure 2M). These results indicate that FKBP25 promotes mitotic entry. Experiments showing reduced apoptosis and increased cell viability in FKBP25 knockdown cells treated with agents of genotoxic stress provide further support for an enhanced G2/M checkpoint (Supplementary Figure S4). Additionally, when these cells are synchronized at the G2/M border and treated with the DNA damage inducing drug etoposide before release, they have less cleaved Parp-1, an indicator of apoptosis (Supplementary Figure S4G). We postulate that this is the result of a potentiated G2/M checkpoint, which prevents damaged cells from entering mitosis and undergoing apoptosis.

FKBP25 associates with microtubules

FKBP25-depleted cells have a phenotype of reduced entry into S-phase and mitosis, which is consistent with disrupted MT dynamics (49). Furthermore, we recently identified a collection of cytoskeletal proteins associated with FKBP25 using both IP-mass spectrometry and BioID proximity labeling (50). Given these data, and the well-characterized relationship between FKBPs and the MT network, we were next interested in testing if FKBP25 is a *bona fide* MAP.

To test this hypothesis, we performed confocal imaging of cells stained for α-Tubulin, a primary component of MTs and FKBP25 (Figure 3). We found that the cytoplasmic fraction of FKBP25 partially co-localizes with α-Tubulin (Figure 3A). To understand how FKBP25 may control cel-
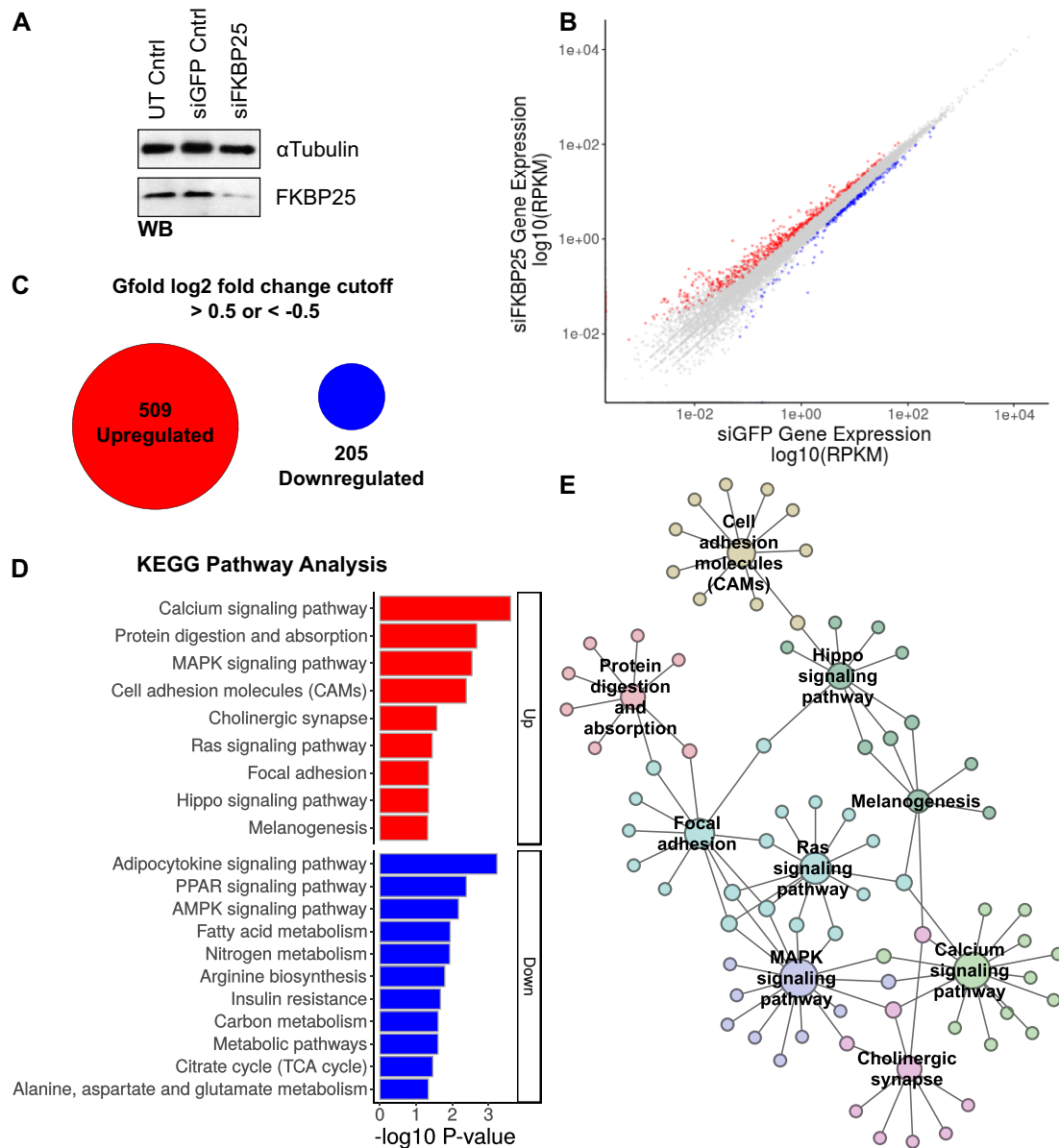
Figure 1. FKBP25 knockdown activates transcriptional networks associated with the stress response and attenuated proliferation. (**A**) siRNA-mediated knockdown of FKBP25 in HEK293 cells relative to untransfected (UT) and GFP-targeting transfected controls. Western blots show protein expression of FKBP25 and an α-Tubulin loading control. (**B**) RNA-Seq transcriptome analysis of cells treated with FKBP25 targeting siRNA versus a GFP targeting control. Expression values are shown as $\log_{10}$ read per kilobase of transcript per million mapped reads (RPKM). Red data points indicate a log2 fold change >0.5 and blue indicates a change <−0.5. (**C**) Number of genes selected for KEGG enrichment analysis based on a log2 fold change of >0.5 (upregulated expression) or <−0.5 (downregulated expression). (**D**) KEGG pathway terms associated with upregulated (red) or downregulated (blue) gene sets identified in B. (**E**) Network depiction of upregulated genes enriched in KEGG pathway analysis; expanded view presented in Supplementary Figure S1.

lular proliferation and entry into mitosis, we followed its localization during the cell cycle by immunofluorescence of asynchronous and M phase synchronized cells (Supplementary Figure S5). During interphase FKBP25 is primarily nuclear with a fraction present in the cytoplasm (Supplementary Figure S5). As prophase begins and chromosomes condense, FKBP25 was excluded from chromatin and maintained this distribution as cells progressed through mitosis. This mitotic localization is reminiscent of proteins that associate with the mitotic spindle apparatus and telophase

midbody (51–53). These cytoskeletal structures, comprised primarily of MT polymers, are the macromolecular machines that segregate chromosomes and coordinate the orientation of the cleavage furrow. Confocal microscopy confirms that FKBP25 colocalizes with the mitotic spindle apparatus during cytokinesis and, as telophase neared its end and daughter nuclei form, FKBP25 returned to chromatin (Figure 3B). These observations demonstrate that FKBP25 interacts with chromatin and the cytoskeleton dynamically. This conclusion is supported by published pro-
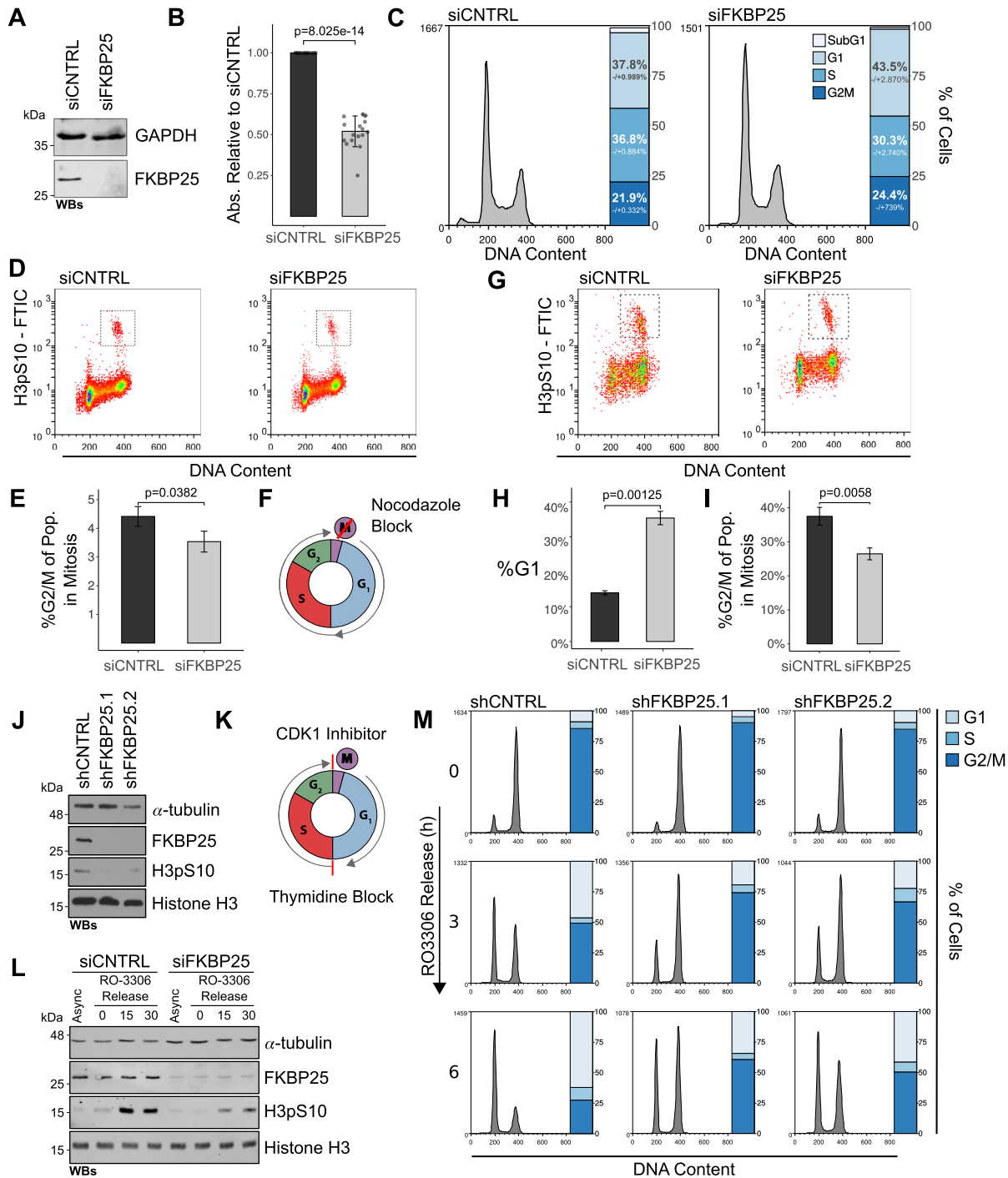
Figure 2. FKBP25 is required for timely progression through the cell cycle. (**A**) Western blot showing FKBP25 knockdown in U2OS cells transfected with siRNAs. GAPDH is shown as a loading control. (**B**) MTT proliferation assay measuring cell viability 72 h post-knockdown. Results shown are the mean ± SD of six independent transfections plated at three densities. (**C–E**) Cell cycle analysis of FKBP25 knockdown cells by flow-cytometry. (C) Histogram of PI-stained cells depicting cell cycle distribution, inlay bar graphs depict the mean ±SD of three replicates. (D) Dot-plot representing fluorescence intensity of H3pS10 levels versus PI-stain. (E) Quantification of H3pS10 positive mitotic cells as a percent of G2/M cells in D. Shown is the mean ±SD for three replicates. (**F**) Schematic representation of nocodazole trap; cells incubated for 8 h in nocodazole to halt progression into G1 of the cell cycle. (**G–I**) Flow cytometry analysis of 8 h nocodazole-trapped cells. (G) Dot-plot of H3pS10 expression versus PI-staining. (H) Quantification of cells remaining in G1. Results are shown as the mean ±SD of three replicates. (I) Percentage of G2/M cells in mitosis. Results are presented as the mean ±SD of three replicates. (**J**) Western blot analysis of mitotic entry 8 h post-nocodazole trap of stable FKBP25 shRNA knockdown U2OS cells. Histone H3 and α-tubulin are shown as loading controls. (**K**) Schematic representation of synchronization at G2/M border by thymidine block followed by CDK1 inhibition (RO3306). (**L**) Western blot analysis of mitotic entry in siRNA transfected cells released from G2/M transition block. (**M**) Flow cytometry analysis of PI-stained stable shRNA FKBP25 knockdown cells released from G2/M transition block.
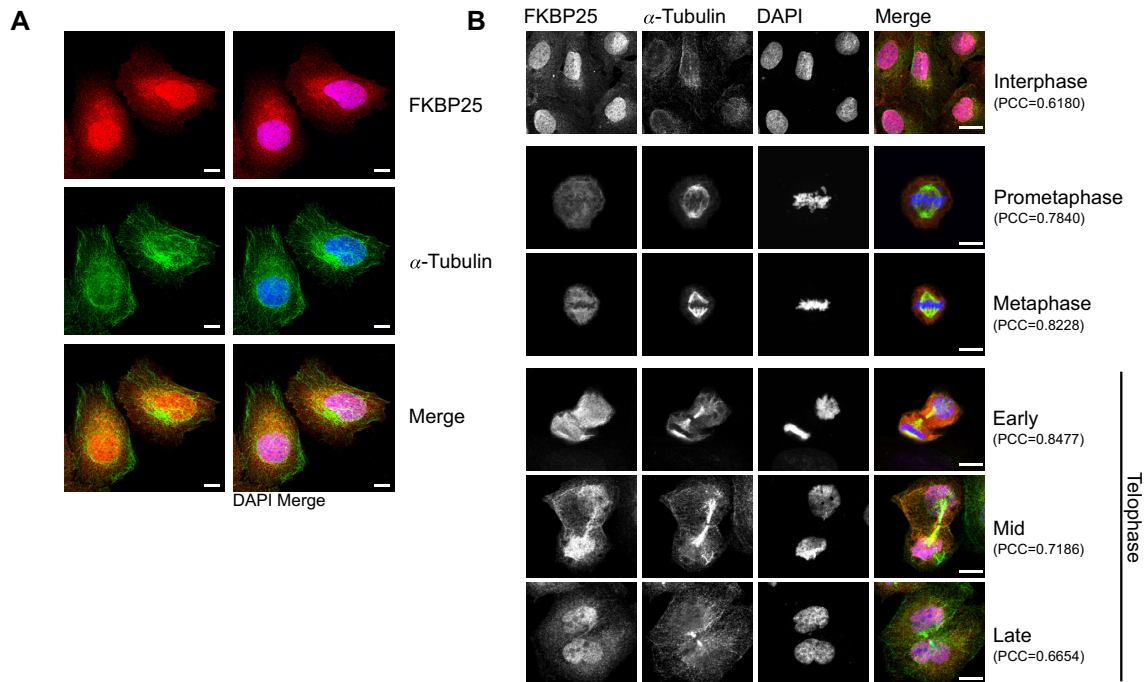
Figure 3. FKBP25 colocalizes with MTs. (**A** and **B**) Confocal imaging of the cellular distribution of FKBP25 (red) and α-Tubulin (green) during (A) interphase and (B) throughout mitosis. Chromosomes stained with DAPI (blue). The co-localization of FKBP25 and tubulin was quantified by Pearson's Correlation Co-efficient (PCC) scores, which take both pixel location and intensity into account to provide a measure of co-distribution, from −1 (mutual exclusion) to 1 (perfect colocalization). Scale bars represent 10 um.

teomic datasets that have identified FKBP25 on purified mitotic spindles from Chinese hamster ovary cells (54) and HeLa S3 cells (35), as well as or own proteomics efforts (31,50). Interestingly, each of these reports also found a significant number of nucleolar and ribosomal proteins associated with the mitotic spindle, suggesting a link between the nucleolus, RNA and MT dynamics. Several of these factors have been further shown to regulate MT dynamics, including nucleolin, NPM1 and RPS3 (37,55,56). Thus, we hypothesized that FKBP25 could play a similar role in the regulation of MT dynamics.

FKBP25 promotes microtubule polymerization independent of catalytic activity

To test this hypothesis and biochemically support our immunofluorescence experiments, we performed MT protein spin-down assays to evaluate binding of FKBP25 to taxol-stabilized MTs. We show that FKBP25 can interact with MTs purified from asynchronous or mitotic HeLa S3 cells as a fraction of recombinant FKBP25 pellets in the presence of MTs compared to a bovine serum albumin negative control, which does not (Figure 4A). To determine which region of the protein was responsible for the interaction with polymerized MTs binding assays were repeated with domain constructs comprising either the N-terminal BTHB domain and linker region or the C-terminal FKBP isomerase domain (Figure 4B). We found that the FKBP prolyl isomerase domain and not the BTHB domain associated with polymerized MT pellets. We next tested whether prolyl isomerase activity or features of the catalytic pocket influence this interaction using a previously characterized

Y198F catalytic null mutant (57) or pre-incubation with rapamycin, a potent low nM affinity FKBP inhibitor (58) (Figure 4C and D). Neither mutational nor chemical disruption of the catalytic pocket altered FKBP25 binding to MTs. These data indicate an alternative surface on the FKBP isomerase domain facilitates contact with MTs. To determine if this interaction has functional consequences, we included recombinant FKBP25 in *in vitro* MT polymerization assays and found that both full-length FKBP25 and a catalytically inert Y198F mutant strongly promote the assembly of tubulin to MTs (Figure 4E). As expected, this effect is mediated by the carboxyl terminal FKBP domain, and not the amino terminal BTHB domain, which we recently showed is a novel double-stranded RNA binding module (50). Together these *in vitro* data define the FKBP domain of FKBP25 as MT binding domain that directly promotes the polymerization of MTs.

We next set out to examine if FKBP25 alters the stability of MTs in cells by performing in cell tubulin polymerization assays. To confirm that any observed phenotypes were not a result of off-target RNAi effects and to test a requirement for prolyl isomerase activity, we generated stable cell lines harboring either catalytically active or inactive tetracycline-inducible transgenes with silent mutations in the siRNA targeting sequence (Figure 5A). We assayed MT stability by immunostaining for α-Tubulin in knockdown/rescue cells extracted with detergent to release the dynamic MT fraction (Figure 5B). Quantification of fluorescence intensity per cell showed a significant disruption in the MT network in the absence of FKBP25, demonstrating that FKBP25 forms a stabilizing interaction with MTs (Figure 5C). This pheno-
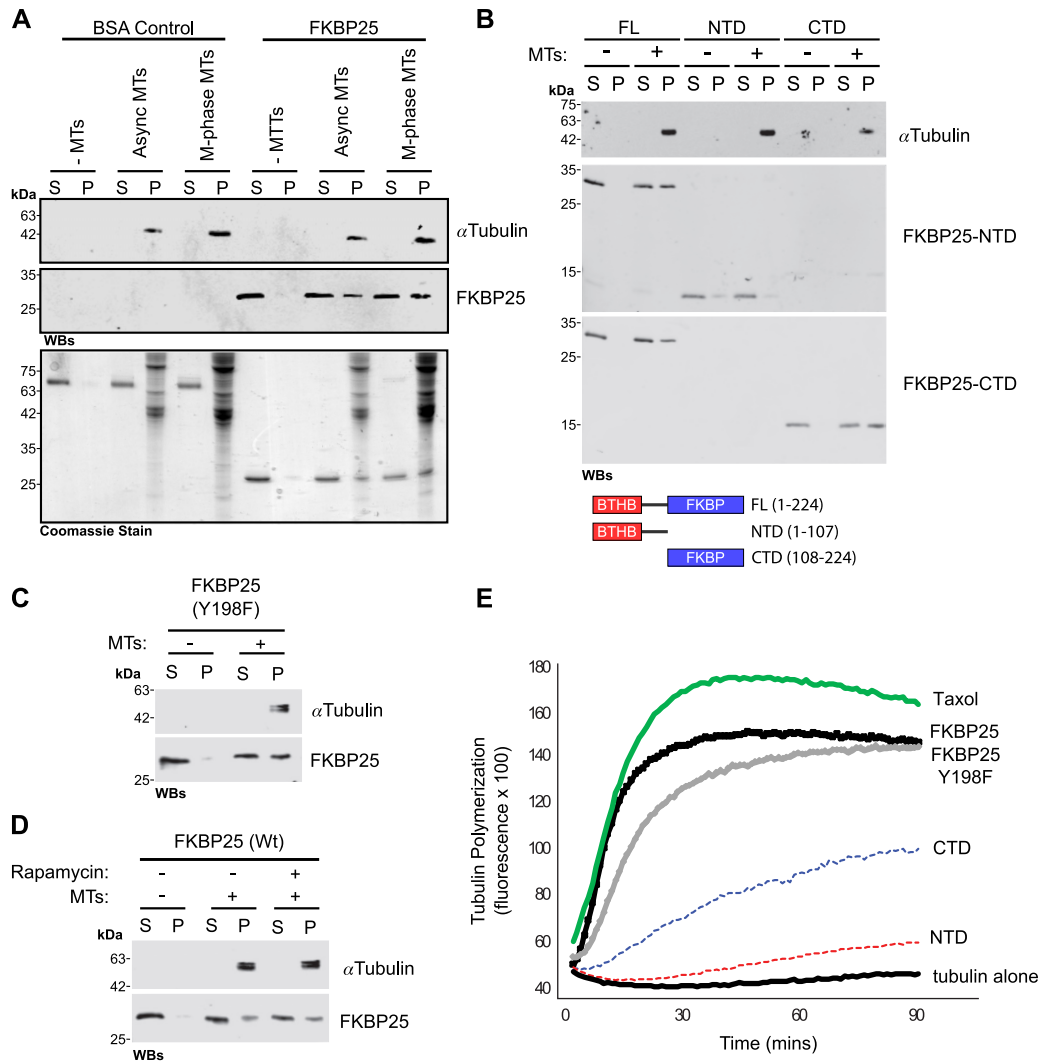
Figure 4. FKBP25 binds polymerized MTs via its FKBP domain. (**A**) *In vitro* MT spin-down assay. Coomassie stained gels and western blots show supernatant (S) and pellet (P) in the absence or presence of MTs purified from asynchronous or mitotic HeLa S3 cells incubated with recombinant FKBP25 or BSA control and centrifuged over a sucrose cushion. (**B** and **D**) Western blots analysis of MT spin-down assay. MT incubated with (**B**) full-length, N-terminal and C-terminal domains of FKBP25, (**C**) a catalytic-null FKBP25 mutant (Y198F) or (**D**) in the presence/absence of 20 nM rapamycin. (**E**) Tubulin polymerization assays. Tubulin polymerization was monitored using a fluorescence based kit (Cytoskeleton, BK011P) in the presence of 3 μM Paclitaxel (Taxol) or 6 μM of the indicated purified recombinant 6-his tagged FKBP25 proteins.

type was rescued by induction of either the wild-type or catalytic null transgenes, demonstrating that while FKBP25 does influence MT dynamics, this function is not dependent on catalytic activity (Figure 5C). We further validated FKBP25's involvement in promoting MT stability using a pelleting assay to separate dynamic MTs (S—soluble fraction) from stable MTs (P—pelleted fraction). In agreement with the immunofluorescence-based assay, we found that stable shRNA knockdown cells had reduced levels of stabilized MTs relative to control shRNA cells (Figure 5D and E). Together, these data support a role for FKBP25 as an MT-stabilizing factor independent of catalytic activity.

Formation of the mitotic spindle apparatus relies on the coordination of multiple pathways to ensure the faithful segregation of chromosomes and genomic integrity (59). Misregulation of these pathways is associated with many pathologies, including cancer. One phenotype of the aber-

rant execution of nuclear division is an increase in micronuclei (MN), which form as a result of chromosome segregation errors (60). Given FKBP25's influence on MT stability, we quantified the frequency of MN in stable shRNA knockdown cells by DAPI staining (Figure 5F) and found that disruption of FKBP25 led to a significant increase in MN frequency. Mitotic MT structures are not only necessary for segregation of chromosomes but also coordinate cytokinesis. Failure at this stage of cell division results in binucleated tetraploid cells, which have also been shown to contribute to carcinogenesis and chromosomal abnormalities (61). Thus, we next looked at the relative number of binucleated cells in knockdown versus control cells and found FKBP25 represses the formation of binucleated cells (Figure 5G). Finally, in support of a MT-stabilizing role of FKBP25, we observe that FKBP25 depleted cells are resistant to Taxol, a MT-stabilizing drug (Figure 5H). Taken together, these
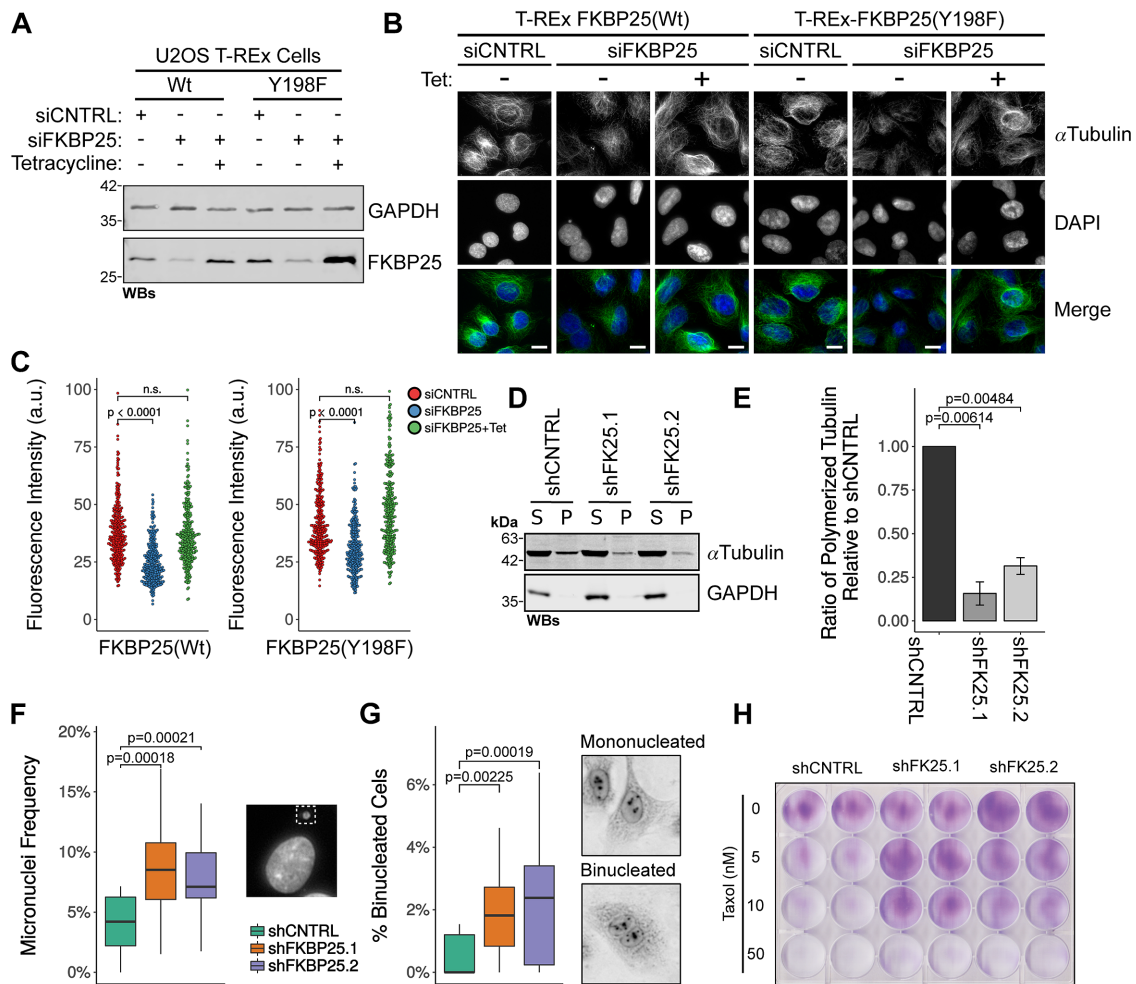
Figure 5. FKBP25 regulates the stability of MTs independent of catalytic activity. (**A**) U2OS Flp-In T-Rex tetracycline inducible knockdown rescue system. Western blot of cells transfected with siRNA and treated with tetracycline to induce expression of either a wild-type or catalytic-null(Y198F) FKBP25 rescue transgene. GAPDH is shown as a loading control. (**B** and **C**) In cell MT stability assay. (**B**) Representative images showing epi-fluorescence microscopy of α-tubulin (green), indicating polymerized MTs and DAPI (blue) showing the nucleus in Flp-In T-Rex U2OS knockdown/rescue cells pre-extracted with PME buffer containing detergent. (C) Quantification of α-tubulin fluorescence intensity per cell (arbitrary units) in B. Plots show the fluorescence intensity measurements of cells from at least five fields of view and >250 cells per sample. (**D**) In cell MT stability pelleting assay. Immunoblot of supernatant and pellet of U2OS stable shRNA knockdown cells permeabilized with PEM buffer containing detergent and centrifuged. Pelleted fraction (P) represents stable polymerized MTs and supernatant (S) unpolymerized tubulin. (**E**) Quantification of immunoblots in D. Results are shown as the mean ±SD for three replicates. (**F**) MN frequency assay. Boxplot showing the frequency of MN in U2OS stable shRNA cells. Measurements are taken from three independent replicates each with at least five fields of view quantified. A representative image of DAPI stained MN relative to the cell nucleus is also shown. (**G**) Quantification of binucleated cells in U2OS stable shRNA-expressing cells visualized by Giemsa staining, as shown in representative images. Boxplot depicts the percentage of binucleated cells in at least five fields of view from three replicate experiments. (**H**) Depletion of FKBP25 renders U2OS cells resistant to Taxol. Stable cell lines expressing the indicated shRNAs were treated with the indicated doses of paclitaxel for 24 h, recovered for 24 h and stained with crystal violet to score viable cells.

results demonstrate that FKBP25's MT-stabilizing activity is critical for formation and attachment of the mitotic spindle apparatus, the coordination of cytokinesis by MTs and ultimately, chromosomal integrity.

FKBP25 is multiply phosphorylated upon entry into mitosis by PKC

We have shown here that FKBP25 is a critical factor in the maintenance of MT stability with implications on mitotic progression and genomic integrity. We were next interested in understanding how this process may be regulated. A wave of phosphorylation coordinates entry into mitosis—large-scale proteomics screens have shown FKBP25 to be phosphorylated at several sites during mitosis (62–64), suggesting a putative regulatory mechanism. To test this, we purified FLAG-tagged FKBP25 from Flp-In HeLa S3 cells synchronized in various stages of the cell cycle and performed PhosTag gel shift western blots probing for FKBP25 (Figure 6A and B). PhosTag is a commercially available phosphate binding tag that can be incorporated into SDS-PAGE gels, resulting in a mobility shift for phosphoproteins (65). Cells synchronized in M-phase by thymidine-nocodazole block showed a hyperphosphorylated form of FKBP25, supporting published evidence of mitotic phosphorylation. To refine the timing of this phosphorylation
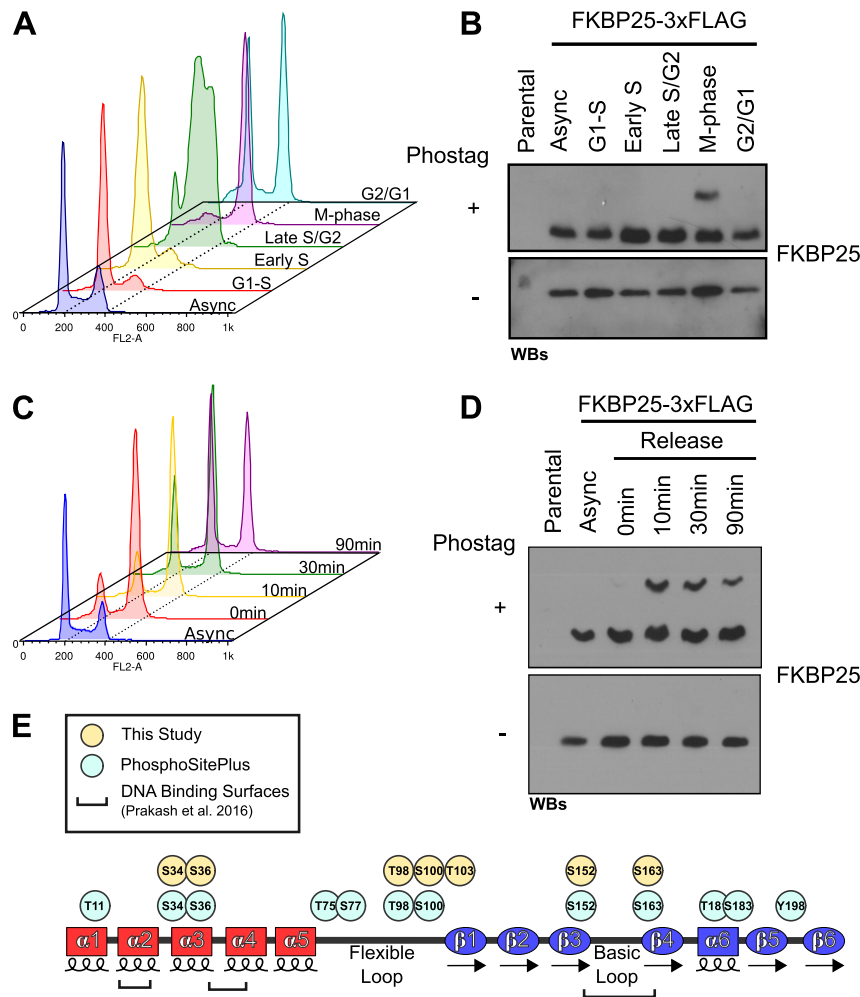
Figure 6. FKBP25 is multiply phosphorylated upon entry into mitosis. (**A**) Cell cycle distribution of synchronized cells. Flow cytometry analysis of PI-stained synchronized Flp-In HeLa S3 cells expressing FLAG-tagged FKBP25. (**B**) Western blotting of FLAG-FKBP25 immunoprecipitate from synchronized cells on SDS-PAGE gels with or without 50 μM Phos-tag. Parental cell line does not have an integrated FKBP25 transgene. (**C**) Flow cytometry analysis of cell cycle distribution of PI-stained cells synchronized at G2/M border by thymidine/CDK1 block and released. (**D**) Western blot analysis of FLAG-FKBP25 IP material from cells synchronized and released at G2/M transition run on SDS-PAGE gels with or without 50 μM Phos-tag. (**E**) Schematic representation of mass spectrometry identified phosphoresidues in immunoprecipitated FLAG-FKBP25 from thymidine/nocodazole-synchronized mitotic cells (this study), phosphoresidues previously detected as described in the PhosphoSitePlus database (67) and characterized DNA binding surfaces (28) are also shown.

event, we repeated PhosTag gel shift assays on cells arrested at the G2/M border and released (Figure 6C and D). The hyperphosphorylated species of FKBP25 was detected within 10 minutes of release, indicating that phosphorylation occurs upon entry into mitosis. The mitotic phosphorylation of FKBP25 appears to be temporally restricted, as detection of the phospho-species decreased at later time points. Mass spectrometry analysis of FLAG-tagged purified FKBP25 from mitotic cells identified seven M-phase phosphorylation sites; S34, S36, T98, S100, T103, S152 and S163 (Figure 6E and Supplementary Figure S6). Except for T103, these sites have all been previously identified (Figure 5E) (66). Interestingly, several of these sites lie proximal to residues involved in the nucleic acid binding activity by FKBP25.

Multiple kinases coordinate mitosis to regulate nuclear envelope disassembly, chromatin, condensation and for-

mation of the mitotic spindle (32). Unfortunately, bioinformatic identification of putative kinase motifs within FKBP25 did not elicit any high confidence hits. Thus, to identify the mitotic FKBP25 kinase, we turned to an unbiased biochemical approach utilizing recombinant FKBP25 as a substrate, kinase-active mitotic extracts and characterized inhibitors of mitotic kinases. Mitotic kinase activity was confirmed in an extract purified from thymidine-nocodazole synchronized HEK 293 cells based on *in vitro* H3pS10 activity (Figure 7A). We then incubated recombinant FKBP25 deletion constructs with the purified extract in the presence of [γ-32P]ATP and visualized phosphorylation by autoradiography (Figure 7B). Each domain of FKBP25 showed some level of phosphorylation, in agreement with the mass spectrometry analysis, which identified multiple phosphorylation events on the BTHB domain, linker and FKBP domain. Kinase reactions were then re-
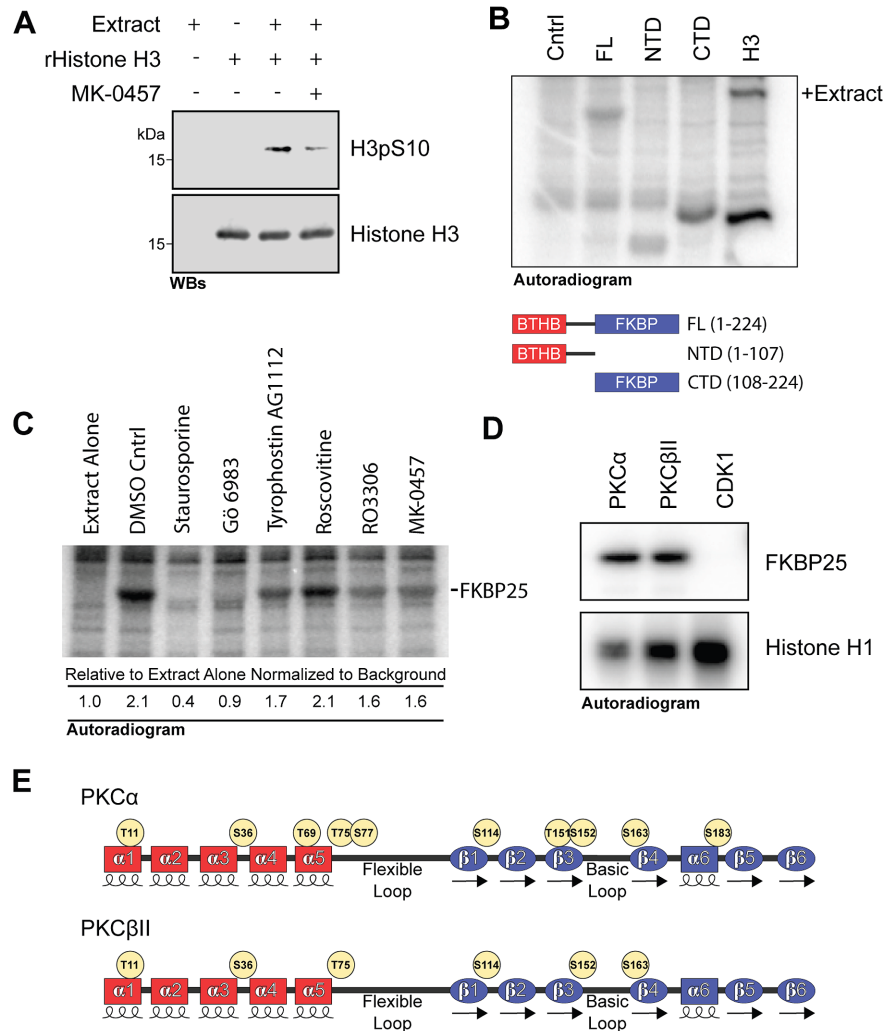
Figure 7. FKBP25 is phosphorylated by PKC. (**A–D**) *In vitro* kinase assays. (A) Western blot analysis of recombinant histone H3 alone, incubated with mitotic extract, or incubated with mitotic extract and the Aurora kinase inhibitor MK-0457 (50 μM) in kinase buffer. (B) Purified full-length proteins were incubated with mitotic extract in the presence of γ[32P]-ATP, resolved by SDS-PAGE and visualized by autoradiography. For the Cntrl lane, no recombinant protein included in the reaction. Histone H3 included as a positive control. (C) Identification of putative mitotic kinase by *in vitro* kinase assay in the presence of mitotic kinase inhibitors. Assays performed as in B with the inclusion of the kinase inhibitors staurosporine (broad range), Gö 6983 (PKC), Tyrphostin AG1112 (CKII), Roscovitine (CDKs), RO3306 (CDK1) and MK-0457(Aurora). (D) *In vitro* kinase assay with recombinant canonical PKC kinases and CDK1. Recombinant FKBP25 incubated with purified PKCα (12.5 ng), PKCβII (12.5 ng) or CDK1-cyclinB1 (20 ng). (**E**) Schematic representation of mass spectrometry identified phosphoresidues on recombinant FKBP25 *in vitro* phosphorylated with either PKCα or PKCβII.

peated in the presence of mitotic kinase inhibitors to decipher the enzyme targeting FKBP25 (Figure 7C). Staurosporine was used as a positive control as it is a potent broad spectrum inhibitor that targets many mitotic kinases (67). Of the selective inhibitors tested, an inhibitor of PKC (Gö 6983) had the most profound effect on FKBP25 phosphorylation. Inhibitors targeting Caesin Kinase II (CKII; tyrphostin AG1112), CDK1-Cyclin B1 (RO3306) and Aurora kinases (MK-0457) showed only modest reductions in phosphorylation, while roscovitine a multipotent cyclin-dependent kinase inhibitor less potent than RO33006 with respect to CDK1 had no effect. The modest effects of several of these inhibitors may represent inhibition of the kinase extract generally and not direct targeting of FKBP25.

PKC is a family of serine/threonine protein kinases consisting of eight isozymes. Increased diacylglycerol, a lipid second messenger, activates the novel isoforms (PKC δ, ε, θ and η), whereas the canonical PKC isozymes (PKCα, βI, βII and γ) also require Ca^{2+} (68). These proteins have a broad range of substrates and are implicated in diverse cellular functions. The PKCβII isozyme has been shown to translocate to the nucleus during G2/M (69). Here PKCβII aids in the disassembly of nuclear envelope by phosphorylation of lamin B (70) and is required for G2/M transition of the cell cycle (71). This event coincides with a rise in nuclear levels of diacylglycerol (69) and increased Ca^{2+} signaling (72), suggesting the importance of canonical PKC signaling in mitotic regulation. Thus, we selected two canonical PKC isoforms, α and βII, to validate PKC phosphorylation of FKBP25 by *in vitro* kinase assays. These experiments show that FKBP25 is phosphorylated by canonical PKC isozymes, but not CDK1 (Figure 7D). Recombinant

histone h1 is shown as a positive control, as it is the target of robust phosphorylation by both PKC and CDK1 (38). We next determined the sites on FKBP25 that are targeted by PKC using mass spectrometry analysis of *in vitro* phosphorylated FKBP25. We found PKC could phosphorylate many of sites identified on FKBP25 purified from mitotic cells, with the exceptions of S36 in the BTHB domain and T98, S100, T103 in the linker region (Figure 7E). This result implies other kinases target FKBP25 during mitosis. One possibility is CKII, which has been previously shown to associate with and phosphorylate FKBP25 (30). However, others have found CKII activity against FKBP25 to be minimal (73). In agreement with this finding, we also show only minimal activity against FKBP25 as compared to PKC *in vitro* (Supplementary Figure S7). However, it is possible CKII phosphorylation of FKBP25 requires additional complex members or there is a requirement for initializing phosphorylation events to prime CKII activity toward FKBP25.

Phosphorylation of FKBP25 disrupts DNA binding but not MT interaction

Our immunofluorescence data demonstrated that FKBP25 is displaced from chromatin early in mitosis and then associates with the forming mitotic spindle. Thus, we next set out to test if phosphorylation during mitosis could influence either nucleic acid binding of FKBP25, as this is a likely determinant of its interactions with chromatin or the novel association with MTs we have uncovered here. To test this, we *in vitro* phosphorylated FKBP25 using either PKCα or PKCβII and performed MT spin-down assays as before and DNA mobility shift assays using a 1:100 DNA-FKBP25 molar ratio, as previously described (Figure 8A and B) (26). We found that phosphorylation of FKBP25 reduced binding of FKBP25 to DNA, as indicated by an increase in the unbound species when incubated with kinase and ATP (Figure 8A). This observation is not particularly surprising, as several of the phosphosites identified lie adjacent to features implicated in the recognition of nucleic acids by FKBP25 (26). In contrast, phosphorylation seemed to have little effect on FKBP25's interaction with polymerized MTs (Figure 8B). We validated these results by repeating these experiments with FKBP25 mutants containing phosphomimetic serine/threonine to glutamate mutations at the sites identified to be phosphorylated by mass spectrometry in mitotic HeLa S3 cells. In agreement with Figure 8B, an $8 \times$ S/T to E mutant, associates with MTs as well as WT FKBP25, confirming these positions do not affect MT association. However, this mutant has a dramatic reduction in DNA binding (Figure 8D). These results support a model where separate surfaces of FKBP25 mediate interactions with DNA and MTs. Characterization of phosphomimetic mutations in either the BTHB domain, linker or FKBP domain revealed that while all mutants showed decreased interaction with DNA, phosphorylation at sites flanking the basic loop of the FKBP domain had the strongest influence on DNA binding (Figure 8D). This observation is in agreement with the NMR characterization of FKBP25–DNA interactions, which showed several sites in the N and C-terminal to be involved in DNA binding (26). Interestingly, single S152E or

S163E mutations showed similar decreases in DNA binding to the double mutant, suggesting that a single phosphorylation event can substantially disrupt FKBP25–DNA interactions (Figure 8E). These results imply that the basic loop contained within the FKBP domain is the primary determinant of FKBP25–DNA contacts; in support of this, we found the FKBP domain alone showed greater binding to DNA than the BTHB domain + linker region (Figure 8F). Interestingly, this stretch of basic residues is unique to the FKBP domain of FKBP25 and is highly conserved in vertebrates (Supplementary Figure S8). These experiments support a model in which mitotic phosphorylation of FKBP25 displaces it from DNA without altering its association with MTs and role in stabilizing the mitotic spindle (Figure 9A).

DISCUSSION

Here we identify the FKBP25 immunophilin as a novel MAP that promotes MT polymerization. We show that FKBP25 dynamically interacts with chromatin and MTs, and this is firmly supported by our analysis of FKBP25 protein interactions using two complementary methodologies (50). Cells lacking FKBP25 display hallmark MT defects including cell cycle delays, and accumulation of both MN and binucleated cells. In terms of the FKBP family, FKBP25 has a unique ability to bind nucleic acids and MTs, with the former regulated during the cell cycle by PKC phosphorylation. This modification is restricted to early mitosis, with phosphorylation disrupting DNA but not MT binding. This study has thus uncovered an additional FKBP MAP, and revealed a novel mechanism of immunophilin regulation.

The DNA binding property of FKBP25 implies that this enzyme may participate in the regulation of DNA transactions, including transcription (24,26,28). We demonstrate here that depletion of FKBP25 has minimal effects on bulk transcription, at least in HEK293 cells. The changes we do observe in the transcriptomes of FKBP25-depleted cells are modest and include an upregulation of MAPK stress response pathway components. MAPK signaling is intrinsically linked to the MT network, with an estimated one-third of MAPK proteins physically associating with the MT cytoskeleton (74). Further, MT disassembly is proposed to activate p38 MAPK signaling leading to inhibition of the cdc25B phosphatase and delayed entry into mitosis (75). Since we find FKBP25 knockdown destabilizes the MT network, the transcriptional changes and cell cycle delays we observe in these cells are likely consequences of MT defects. It is important to note that we cannot completely rule out a direct role for FKBP25 in transcriptional control, and further research is required to determine FKBP25's role in the regulation of chromatin. One potential explanation for FKBP25's conserved nucleic acid binding feature is that this is a means to regulate FKBP25's MT-stabilizing activity during interphase by promoting nuclear localization. In this way a pool of FKBP25 may operate similar to, the mitotic spindle associated proteins NuSAP, NuMa and TPX2, which show a cell cycle-dependent localization, localizing to the nucleus during interphase to limit their MT-stabilizing activities until mitotic breakdown of the nuclear envelope (76–79). Further, TPX2-mediated MT nucleation is inhib-
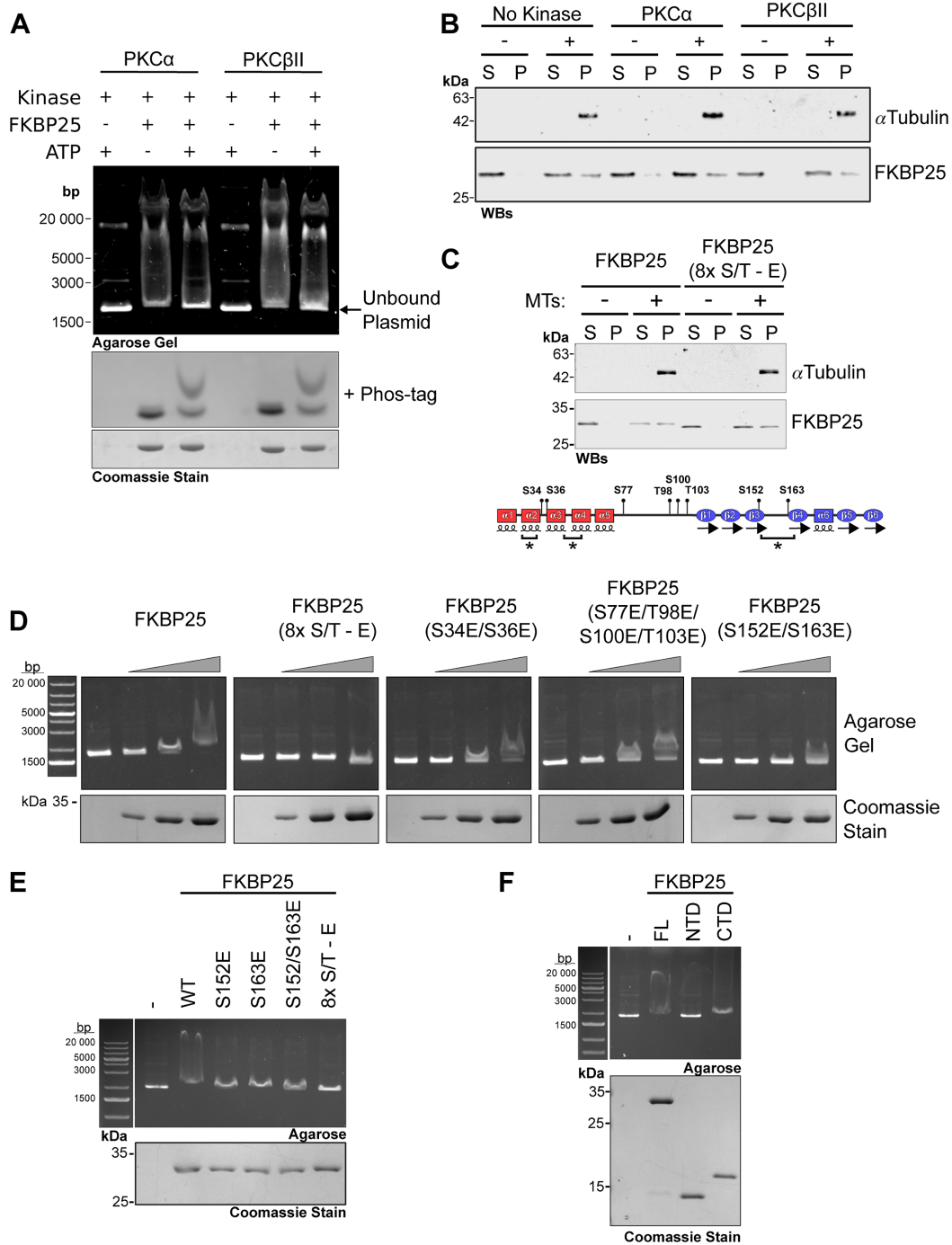
Figure 8. Phosphorylation of FKBP25 impairs DNA binding, but not its interaction with MTs. (**A**) Gel retardation assay measuring DNA binding of FKBP25 with and without *in vitro* PKC phosphorylation. Coomassie stained SDS-PAGE gels with or without 50 μM Phos-tag show loading and phosphorylation status of FKBP25. (**B**) *In vitro* MT spin-down binding assay with recombinant FKBP25 *in vitro* phosphorylated with PKCα or PKCβII. No kinase sample is shown as a control. (**C**) *In vitro* MT spin-down assay with phosphomimetic recombinant FKBP25 8xS/T to E mutant (S32, S36, S77, T98, S100, T103, S152, S163 mutated to glutamate). (**D**–**F**) Gel retardation assay measuring DNA binding of recombinant FKBP25 (D and E) wild-type sequence and phosphomimetic S/T to E mutants, and (F) FKBP25 domains.
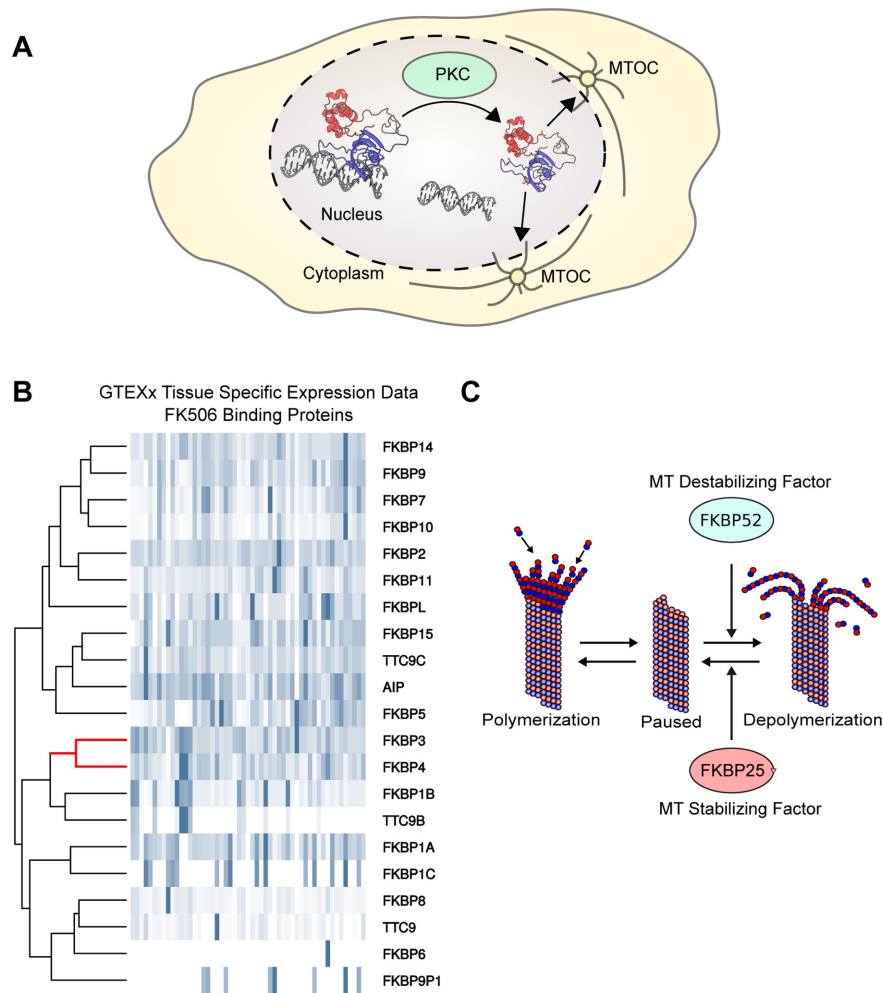
Figure 9. Model depicting the involvement of FKBP25 in MT stability. (**A**) Model. FKBP25 (PDB ID: 2MPH) is phosphorylated by PKC during mitosis to promote its release from chromatin, freeing FKBP25 to function as a MT stabilizer in the formation of the mitotic spindle apparatus. (**B**) Heatmap of normalized tissue-specific gene expression from GTEx datasets for human FKBP domain containing proteins. FKBP52 (FKBP4) and FKBP25 (FKBP3) cluster together based on tissue-specific expression patterns, indicated in red. (**C**) Schematic representation of opposing functions of FKBP52 and FKBP25 on MT stability.

ited by importins, nuclear import proteins (80). FKBP25 contains a putative nuclear localization signal (30), however direct binding to importins has not been shown. As FKBP25 is a relatively small protein (25 kDa), it may enter the nucleus by diffusion and its nucleic acid binding properties would act to support its residency there. However, it is important to note that functions in MT dynamics and chromatin biology are not mutually exclusive. Interestingly, a number of chromatin regulatory proteins have been shown to moonlight as chromatin-dissociated MAPs (81). Therefore, FKBP25's role in chromatin biology warrants further investigation.

Cell cycle regulation and MT dynamics are intricately coupled. Consistent with the cell cycle phenotype in FKBP25 depleted cells, disruption of MT dynamics has also been shown to attenuate G1/S and G2/M transitions (49) and interfere with initiation of mitosis (82,83). During mitosis MT dynamics increase, and the interphase MT network undergoes a dramatic rearrangement to form the mitotic spindle apparatus (84). This process is tightly regulated

by MAPs and a primary cause of chromosomal instability is a failure of the mitotic spindle (85). We find that FKBP25 is multiply phosphorylated in mitosis and identify PKC as one mitotic kinase responsible. PKC-mediated phosphorylation blocks DNA binding and releases FKBP25 from chromatin increasing the available pool to bind to MTs during formation of the mitotic spindle. Interestingly, PKC activity has been previously linked to the regulation of MT dynamics, where activation of PKC by DAG-lactone treatment increased MT dynamics and reduced MT catastrophe through phosphorylation of α-tubulin (86). In line with FKBP25 regulating MT dynamics during mitosis we found FKBP25 co-localized with the mitotic spindle apparatus. Also, decreased expression of FKBP25 led to an increase in MN, presumably caused by mis-segregation of chromosomes and increased numbers of binucleated cells, suggesting a failure to complete cytokinesis. Collectively, these observations show that FKBP25's role in regulating MT dynamics during mitosis is required for the stability of the genome during cell division. In support of our re-

sults FKBP25 was found to co-purify with MTs by several groups (35,54,87).

FKBP family members are known to interact with both MTs and MAPs. Of particular note is FKBP52, a large immunophilin that, like FKBP25, can bind the MT network through its FKBP domain (20,88). However, the binding of these two FKBPs to MTs has the opposite effect: FKBP52 inhibits MT polymerization (17), and we show here that FKBP25 binding promotes MT polymerizartion. Notably, FKBP52 and FKBP25 are co-expressed in multiple tissues and share a similar tissue-specific expression pattern (Figure 9B and C). Like FKBP52, FKBP25 is enriched in neurons in the brain (89). These observations raise the possibility that these two FKBPs may act antagonistically in the regulation of MT dynamics.

The MAP protein Tau is central to the etiologies of protein aggregation tautopothies such as Alzheimer's and Parkinson's diseases. FKBP52 is known to bind Tau and this interaction promotes aggregation independently of prolyl isomerase activity (90–93). FKBP25 may also influence Tau. A recent unbiased proteomic search for factors associated with Tau identified FKBP25 (referred to by its gene name FKBP3 in this report) and not FKBP52 as the predominant FKBP in the Tau interactome (94). Interestingly, the Tau interactome is highly similar to that of FKBP25 (31,50): both proteins co-purify with similar sets of RNA and DNA binding proteins including components of the large ribosomal subunit, several RNA binding and processing factors, and histone H1. Furthermore, a large-scale screen identified FKBP25 as a direct mRNA binding protein (95) and we have recently identified FKBP25's N-terminal BTHB domain as a novel dsRNA binding module that recruits FKBP25 to ribonucleoproteins (50). Collectively, these observations establish FKBP25 as a bridge between RNA and the cytoskeleton that should be further investigated. The precedent for such a connection is already established from reports of ribosomal proteins, NPM and NCL associating with MTs (37,55,56). Notably, these are also FKBP25 interactors (31,50). Future investigations addressing the impact of FKBP25 on both Tau (mis)function and transport of RNA cargo in neuronal cells is thus warranted.

A fundamental assumption about prolyl isomerases is that they influence biology through catalytic isomerization of prolines in substrate proteins. While there are good examples to support this model (9,10,96,97), a growing body of literature demonstrates that these proteins also have non-catalytic impacts on biological processes, presumably via direct binding events (27,28,98,99). For example, we recently showed that the FKBP domain of yeast Fpr4, which can target histone prolines (10,100) could also affect chromatin fiber self-association independently of catalytic function (101). This illustrates that targets of catalytic action may reside close to or within binding partners of FKBPs. As already mentioned, FKBP52's ability to destabilize MTs is independent of its prolyl isomerase activity (91) and two catalytically inactive FKBPs, FKBPL and FKBP15, function in the MT-directed transport of signaling molecules (21,22). Thus, the catalytic activity of FKBP domains is not a prerequisite for associating with, and regulating, macromolecular complexes, including those of the MT network. While

the mechanism of FKBP25 impact on MT polymerization appears to be non-catalytic this does not mean that there is no function for its prolyl isomerase activity. On the contrary; the retention and conservation of catalytic residues in FKBP25, and in FKBP52, indicates that these enzymes likely do have proline targets, and based on proximity alone, the MT network is a good place to look for them. Owing to the inherent reversibility of *cis-trans* proline switches, it will be critical to monitor the impact of FKBPs on MT polymerization, MT–MAP interactions, and transport of cargoes with methodologies sensitive to the dynamics of these processes.

Understanding how FKBPs impact the cytoskeleton in neuronal cells is especially relevant because neuroimmunophilins are promising targets in the treatment of MT-associated diseases such as Alzheimer's and Parkinson's (23,102,103). This is the first report to comprehensively describe the biological impacts of the nucleic-acid binding immunophilin, FKBP25. Our results provide new insight into its function by identifying this protein as a *bona fide* and dynamically regulated MAP and RNA binding protein (50). These data, and the observations that FKBP25 is highly enriched in neurons and interacts with pathogenic Tau forms, provide justification for the inclusion of FKBP25 in future investigations of neuroimmunophilins, MTs and protein mis-folding tautopathies.

DATA AVAILABILITY

RNA-seq data have been deposited in NCBI'S Gene Expression Omnibus database (GSE100813).

SUPPLEMENTARY DATA

Supplementary Data are available at NAR Online.

Conflict of interest statement. None declared.

REFERENCES

1. Weiss,M.S., Jabs,A. and Hilgenfeld,R. (1998) Peptide bonds revisited. *Nat. Struct. Mol. Biol.*, **5**, 676–676.
2. Stewart,D.E., Sarkar,A. and Wampler,J.E. (1990) Occurrence and role of cis peptide bonds in protein structures. *J. Mol. Biol.*, **214**, 253–260.
3. Göthel,S.F. and Marahiel,M.A. (1999) Peptidyl-prolyl cis-trans isomerases, a superfamily of ubiquitous folding catalysts. *Cell. Mol. Life Sci.*, **55**, 423–436.
4. Chelu,M.G., Danila,C.I., Gilman,C.P. and Hamilton,S.L. (2004) Regulation of ryanodine receptors by FK506 binding proteins. *Trends Cardiovasc. Med.*, **14**, 227–234.
5. Brichkina,A., Nguyen,N.T.M., Baskar,R., Wee,S., Gunaratne,J., Robinson,R.C. and Bulavin,D. V (2016) Proline isomerisation as a novel regulatory mechanism for p38MAPK activation and functions. *Cell Death Differ.*, **23**, 1592–1601.
6. Lu,K.P., Finn,G., Lee,T.H. and Nicholson,L.K. (2007) Prolyl cis-trans isomerization as a molecular timer. *Nat. Chem. Biol.*, **3**, 619–629.
7. Sarkar,P., Reichman,C., Saleh,T., Birge,R.B. and Kalodimos,C.G. (2007) Proline cis-trans isomerization controls autoinhibition of a signaling protein. *Mol. Cell*, **25**, 413–426.
8. Hanes,S.D. (2015) Prolyl isomerases in gene transcription. *Biochim. Biophys. Acta*, **1850**, 2017–2034.
9. Dilworth,D., Gudavicius,G., Leung,A. and Nelson,C.J. (2012) The roles of peptidyl-proline isomerases in gene regulation. *Biochem. Cell Biol.*, **90**, 55–69.
10. Nelson,C.J., Santos-Rosa,H. and Kouzarides,T. (2006) Proline isomerization of histone H3 regulates lysine methylation and gene expression. *Cell*, **126**, 905–916.
11. Wang,Z., Song,J., Milne,T.A., Wang,G.G., Li,H., Allis,C.D. and Patel,D.J. (2010) Pro isomerization in MLL1 PHD3-Bromo cassette connects H3K4me readout to CyP33 and HDAC-mediated repression. *Cell*, **141**, 1183–1194.
12. Yao,Y.L., Liang,Y.C., Huang,H.H. and Yang,W.M. (2011) FKBPs in chromatin modification and cancer. *Curr. Opin. Pharmacol.*, **11**, 301–307.
13. Wang,Y. and Mandelkow,E. (2015) Tau in physiology and pathology. *Nat. Rev. Neurosci.*, **17**, 22–35.
14. Nakamura,K., Greenwood,A., Binder,L., Bigio,E.H., Denial,S., Nicholson,L., Zhou,X.Z. and Lu,K.P. (2012) Proline isomer-specific antibodies reveal the early pathogenic tau conformation in Alzheimer's disease. *Cell*, **149**, 232–244.
15. Lu,P.J., Wulf,G., Zhou,X.Z., Davies,P. and Lu,K.P. (1999) The prolyl isomerase Pin1 restores the function of Alzheimer-associated phosphorylated tau protein. *Nature*, **399**, 784–788.
16. Koren,J., Jinwal,U.K., Davey,Z., Kiray,J., Arulselvam,K. and Dickey,C.A. (2011) Bending tau into shape: the emerging role of peptidyl-prolyl isomerases in tauopathies. *Mol. Neurobiol.*, **44**, 65–70.
17. Chambraud,B., Belabes,H., Fontaine-Lenoir,V., Fellous,A. and Baulieu,E.E. (2007) The immunophilin FKBP52 specifically binds to tubulin and prevents microtubule formation. *FASEB J.*, **21**, 2787–2797.
18. Galigniana,M.D., Morishima,Y., Gallay,P.A. and Pratt,W.B. (2004) Cyclophilin-A is bound through its peptidylprolyl isomerase domain to the cytoplasmic dynein motor protein complex. *J. Biol. Chem.*, **279**, 55754–55759.
19. Galigniana,M.D., Harrell,J.M., Murphy,P.J.M., Chinkers,M., Radanyi,C., Renoir,J.M., Zhang,M. and Pratt,W.B. (2002) Binding of hsp90-associated immunophilins to cytoplasmic dynein: Direct binding and in vivo evidence that the peptidylprolyl isomerase domain is a dynein interaction domain. *Biochemistry*, **41**, 13602–13610.
20. Wochnik,G.M., Rüegg,J., Abel,G.A., Schmidt,U., Holsboer,F. and Rein,T. (2005) FK506-binding proteins 51 and 52 differentially regulate dynein interaction and nuclear translocation of the glucocorticoid receptor in mammalian cells. *J. Biol. Chem.*, **280**, 4609–4616.
21. McKeen,H.D., McAlpine,K., Valentine,A., Quinn,D.J., McClelland,K., Byrne,C., O'Rourke,M., Young,S., Scott,C.J.,

McCarthy,H.O. *et al.* (2008) A novel FK506-like binding protein interacts with the glucocorticoid receptor and regulates steroid receptor signaling. *Endocrinology*, **149**, 5724–5734.
22. Viklund,I.M., Aspenström,P., Meas-Yedid,V., Zhang,B., Kopec,J., Ågren,D., Schneider,G., D'Amato,M., Olivo-Marin,J.C., Sansonetti,P. *et al.* (2009) WAFL, a new protein involved in regulation of early endocytic transport at the intersection of actin and microtubule dynamics. *Exp. Cell Res.*, **315**, 1040–1052.
23. Hausch,F. (2015) FKBPs and their role in neuronal signaling. *Biochim. Biophys. Acta*, **1850**, 2035–2040.
24. Rivière,S., Ménez,A. and Galat,A. (1993) On the localization of FKBP25 in T-lymphocytes. *FEBS Lett.*, **315**, 247–251.
25. Galat,A., Thai,R. and Stura,E.A. (2014) Diversified targets of FKBP25 and its complex with rapamycin. *Int. J. Biol. Macromol.*, **69**, 344–352.
26. Prakash,A., Shin,J., Rajan,S. and Yoon,H.S. (2016) Structural basis of nucleic acid recognition by FK506-binding protein 25 (FKBP25), a nuclear immunophilin. *Nucleic Acids Res.*, **44**, 2909–2925.
27. Ochocka,A.M., Kampanis,P., Nicol,S., Allende-Vega,N., Cox,M., Marcar,L., Milne,D., Fuller-Pace,F. and Meek,D. (2009) FKBP25, a novel regulator of the p53 pathway, induces the degradation of MDM2 and activation of p53. *FEBS Lett.*, **583**, 621–626.
28. Yang,W.M., Yao,Y.L. and Seto,E. (2001) The FK506-binding protein 25 functionally associates with histone deacetylases and with transcription factor YY1. *EMBO J.*, **20**, 4814–4825.
29. Helander,S., Montecchio,M., Lemak,A., Farès,C., Almlöf,J., Li,Y., Yee,A., Arrowsmith,C.H., Dhe-Paganon,S. and Sunnerhagen,M. (2014) Basic Tilted Helix Bundle—a new protein fold in human FKBP25/FKBP3 and HectD1. *Biochem. Biophys. Res. Commun.*, **447**, 26–31.
30. Jin,Y.J. and Burakoff,S.J. (1993) The 25-kDa FK506-binding protein is localized in the nucleus and associates with casein kinase II and nucleolin. *Proc. Natl. Acad. Sci. U.S.A.*, **90**, 7769–7773.
31. Gudavicius,G., Dilworth,D., Serpa,J.J., Sessler,N., Petrotchenko,E.V., Borchers,C.H. and Nelson,C.J. (2014) The prolyl isomerase, FKBP25, interacts with RNA-engaged nucleolin and the pre-60S ribosomal subunit. *RNA*, **20**, 1014–1022.
32. Tang,H.M. and Poon,R.Y. (2011) How protein kinases co-ordinate mitosis in animal cells. *Biochem. J*, **435**, 17–31.
33. van de Loosdrecht,A.A., Beelen,R.H.J., Ossenkoppele,G.J., Broekhoven,M.G. and Langenhuijsen,M.M.A.C. (1994) A tetrazolium-based colorimetric MTT assay to quantitate human monocyte mediated cytotoxicity against leukemic cells from cell lines and patients with acute myeloid leukemia. *J. Immunol. Methods*, **174**, 311–320.
34. Schindelin,J., Arganda-Carreras,I., Frise,E., Kaynig,V., Longair,M., Pietzsch,T., Preibisch,S., Rueden,C., Saalfeld,S., Schmid,B. *et al.* (2012) Fiji: an open-source platform for biological-image analysis. *Nat. Methods*, **9**, 676–682.
35. Ozlü,N., Monigatti,F., Renard,B.Y., Field,C.M., Steen,H., Mitchison,T.J. and Steen,J.J. (2010) Binding partner switching on microtubules and aurora-B in the mitosis to cytokinesis transition. *Mol. Cell. Proteomics*, **9**, 336–350.
36. Sloboda,R.D. (2015) Isolation of microtubules and microtubule-associated proteins using paclitaxel. *Cold Spring Harb. Protoc.*, **2015**, 152–154.
37. Wang,G., Gao,X., Huang,Y., Yao,Z., Shi,Q. and Wu,M. (2010) Nucleophosmin/B23 inhibits Eg5-mediated microtubule depolymerization by inactivating its ATPase activity. *J. Biol. Chem.*, **285**, 19060–19067.
38. Mühlhäusser,P. and Kutay,U. (2007) An in vitro nuclear disassembly system reveals a role for the RanGTPase system and microtubule-dependent steps in nuclear envelope breakdown. *J. Cell Biol.*, **178**, 595–610.
39. Laurell,E., Beck,K., Krupina,K., Theerthagiri,G., Bodenmiller,B., Horvath,P., Aebersold,R., Antonin,W. and Kutay,U. (2011) Phosphorylation of Nup98 by multiple kinases is crucial for NPC disassembly during mitotic entry. *Cell*, **144**, 539–550.
40. Franken,N.a.P., Rodermond,H.M., Stap,J., Haveman,J. and van Bree,C. (2006) Clonogenic assay of cells in vitro. *Nat. Protoc.*, **1**, 2315–2319.
41. Guzman,C., Bagga,M., Kaur,A., Westermarck,J. and Abankwa,D. (2014) ColonyArea: an ImageJ plugin to automatically quantify colony formation in clonogenic assays. *PLoS One*, **9**, e92444.

42. Kim,D., Langmead,B. and Salzberg,S.L. (2015) HISAT: a fast spliced aligner with low memory requirements. *Nat. Methods*, **12**, 357–360.
43. Feng,J., Meyer,C.A., Wang,Q., Liu,J.S., Liu,X.S. and Zhang,Y. (2012) GFOLD: a generalized fold change for ranking differentially expressed genes from RNA-seq data. *Bioinformatics*, **28**, 2782–2788.
44. Huang,D.W., Lempicki,R. and Sherman,B.T. (2009) Systematic and integrative analysis of large gene lists using DAVID bioinformatics resources. *Nat. Protoc.*, **4**, 44–57.
45. Yu,G., Wang,L.-G., Han,Y. and He,Q.-Y. (2012) clusterProfiler: an R package for comparing biological themes among gene clusters. *Omi. A J. Integr. Biol.*, **16**, 284–287.
46. Ahn,J., Murphy,M., Kratowicz,S., Wang,A., Levine,a.J. and George,D.L. (1999) Down-regulation of the stathmin/Op18 and FKBP25 genes following p53 induction. *Oncogene*, **18**, 5954–5958.
47. Agarwal,M.L., Agarwal,A., Taylor,W.R. and Stark,G.R. (1995) p53 controls both the G2/M and the G1 cell cycle checkpoints and mediates reversible growth arrest in human fibroblasts. *Proc. Natl. Acad. Sci. U.S.A.*, **92**, 8493–8497.
48. Rizkallah,R. and Hurt,M.M. (2009) Regulation of the transcription factor YY1 in mitosis through phosphorylation of its DNA-binding domain. *Mol. Biol. Cell*, **20**, 4766–4776.
49. Blajeski,A.L., Phan,V.a, Kottke,T.J. and Kaufmann,S.H. (2002) G 1 and G 2 cell-cycle arrest following microtubule depolymerization in human breast cancer cells. *J. Clin. Invest.*, **110**, 91–99.
50. Dilworth,D., Upadhyay,S.K., Bonnafous,P., Edoo,A.B., Bourbigot,S., Pesek-Jardim,F., Gudavicius,G., Serpa,J.J., Petrotchenko,E.V., Borchers,C.H. *et al.* (2017) The basic tilted helix bundle domain of the prolyl isomerase FKBP25 is a novel double-stranded RNA binding module. *Nucleic Acids Res.*, **45**, 11989–12004.
51. Kim,S.M., Choi,E.J., Song,K.J., Kim,S., Seo,E., Jho,E.H. and Kee,S.H. (2009) Axin localizes to mitotic spindles and centrosomes in mitotic cells. *Exp. Cell Res.*, **315**, 943–954.
52. Ishii,S., Kurasawa,Y., Wong,J. and Yu-Lee,L.-Y. (2008) Histone deacetylase 3 localizes to the mitotic spindle and is required for kinetochore-microtubule attachment. *Proc. Natl. Acad. Sci. U.S.A.*, **105**, 4179–4184.
53. Tegha-Dunghu,J., Neumann,B., Reber,S., Krause,R., Erfle,H., Walter,T., Held,M., Rogers,P., Hupfeld,K., Ruppert,T. *et al.* (2008) Eml3 is a nuclear microtubule-binding protein required for the correct alignment of chromosomes in metaphase. *J. Cell Sci.*, **121**, 1718–1726.
54. Bonner,M.K., Poole,D.S., Xu,T., Sarkeshik,A., Yates,J.R. and Skop,A.R. (2011) Mitotic spindle proteomics in Chinese hamster ovary cells. *PLoS One*, **6**, e20489.
55. Jang,C.Y., Kim,H.D., Zhang,X., Chang,J.S. and Kim,J. (2012) Ribosomal protein S3 localizes on the mitotic spindle and functions as a microtubule associated protein in mitosis. *Biochem. Biophys. Res. Commun.*, **429**, 57–62.
56. Gaume,X., Place,C., Delage,H., Mongelard,F., Monier,K. and Bouvet,P. (2016) Expression of nucleolin affects microtubule dynamics. *PLoS One*, **11**, e0157534.
57. Gudavicius,G., Soufari,H., Upadhyay,S.K., Upadhyay,S., Mackereth,C.D. and Nelson,C.J. (2013) Resolving the functions of peptidylprolyl isomerases: insights from the mutagenesis of the nuclear FKBP25 enzyme. *Biochem. Soc. Trans.*, **41**, 761–768.
58. Jin,Y.J., Burakoff,S.J. and Bierer,B.E. (1992) Molecular cloning of a 25-kDa high affinity rapamycin binding protein, FKBP25. *J. Biol. Chem.*, **267**, 10942–10945.
59. Prosser,S.L. and Pelletier,L. (2017) Mitotic spindle assembly in animal cells: a fine balancing act. *Nat. Rev. Mol. Cell Biol.*, **18**, 187–201.
60. Holland,A.J. and Cleveland,D.W. (2012) Chromoanagenesis and cancer: mechanisms and consequences of localized, complex chromosomal rearrangements. *Nat. Med.*, **18**, 1630–1638.
61. Fujiwara,T., Bandi,M., Nitta,M., Ivanova,E.V., Bronson,R.T. and Pellman,D. (2005) Cytokinesis failure generating tetraploids promotes tumorigenesis in p53-null cells. *Nature*, **437**, 1043–1047.
62. Olsen,J.V., Vermeulen,M., Santamaria,A., Kumar,C., Miller,M.L., Jensen,L.J., Gnad,F., Cox,J., Jensen,T.S., Nigg,E.A. *et al.* (2010) Quantitative phosphoproteomics reveals widespread full phosphorylation site occupancy during mitosis. *Sci. Signal.*, **3**, ra3.
63. Dephoure,N., Zhou,C., Villén,J., Beausoleil,S.A., Bakalarski,C.E., Elledge,S.J. and Gygi,S.P. (2008) A quantitative atlas of mitotic phosphorylation. *Proc. Natl. Acad. Sci. U.S.A.*, **105**, 10762–10767.
64. Kettenbach,A.N., Schweppe,D.K., Faherty,B.K., Pechenick,D., Pletnev,A.a and Gerber,S.a (2011) Quantitative phosphoproteomics identifies substrates and functional modules of Aurora and Polo-like kinase activities in mitotic cells. *Sci. Signal.*, **4**, rs5.
65. Kinoshita,E. (2005) Phosphate-binding tag, a new tool to visualize phosphorylated proteins. *Mol. Cell. Proteomics*, **5**, 749–757.
66. Hornbeck,P. V., Chabra,I., Kornhauser,J.M., Skrzypek,E. and Zhang,B. (2004) PhosphoSite: a bioinformatics resource dedicated to physiological protein phosphorylation. *Proteomics*, **4**, 1551–1561.
67. Karaman,M.W., Herrgard,S., Treiber,D.K., Gallant,P., Atteridge,C.E., Campbell,B.T., Chan,K.W., Ciceri,P., Davis,M.I., Edeen,P.T. *et al.* (2008) A quantitative analysis of kinase inhibitor selectivity. *Nat. Biotechnol.*, **26**, 127–132.
68. Mochly-Rosen,D., Das,K. and Grimes,K. V (2012) Protein kinase C, an elusive therapeutic target? *Nat. Rev. Discov.*, **11**, 937–957.
69. Deacon,E.M., Pettitt,T.R., Webb,P., Cross,T., Chahal,H., Wakelam,M.J.O. and Lord,J.M. (2002) Generation of diacylglycerol molecular species through the cell cycle: a role for 1-stearoyl, 2-arachidonyl glycerol in the activation of nuclear protein kinase C-betaII at G2/M. *J. Cell Sci.*, **115**, 983–989.
70. Goss,V.L., Hocevar,B.A., Thompson,L.J., Stratton,C.A., Burns,D.J. and Fields,A.P. (1994) Identification of nuclear beta II protein kinase C as a mitotic lamin kinase. *J. Biol. Chem.*, **269**, 19074–19080.
71. Thompson,L.J. and Fields,A.P. (1996) beta II protein kinase C is required for the G2/M phase transition of cell cycle. *J. Biol. Chem.*, **271**, 15045–15053.
72. Machaca,K. (2011) Ca2+ signaling, genes and the cell cycle. *Cell Calcium*, **49**, 323–330.
73. Shi,Y., Brown,E.D. and Walsh,C.T. (1994) Expression of recombinant human casein kinase II and recombinant heat shock protein 90 in Escherichia coli and characterization of their interactions. *Proc. Natl Acad. Sci. U.S.A.*, **91**, 2767–2771.
74. Reszka,A.A., Seger,R., Diltz,C.D., Krebs,E.G. and Fischer,E.H. (1995) Association of mitogen-activated protein kinase with the microtubule cytoskeleton. *Proc. Natl. Acad. Sci. U.S.A.*, **92**, 8881–8885.
75. Mikhailov,A., Shinohara,M. and Rieder,C.L. (2005) The p38-mediated stress-activated checkpoint: A rapid response system for delaying progression through antephase and entry into mitosis. *Cell Cycle*, **4**, 57–62.
76. Wittmann,T., Wilm,M., Karsenti,E. and Vernos,I. (2000) TPX2, a novel Xenopus MAP involved in spindle pole organization. *J. Cell Biol.*, **149**, 1405–1418.
77. Merdes,A., Ramyar,K., Vechio,J.D. and Cleveland,D.W. (1996) A complex of NuMA and cytoplasmic dynein is essential for mitotic spindle assembly. *Cell*, **87**, 447–458.
78. Kahana,J.A. (2001) CELL CYCLE: some importin news about spindle assembly. *Science (80-.).*, **291**, 1718–1719.
79. Raemaekers,T., Ribbeck,K., Beaudouin,J., Annaert,W., Van Camp,M., Stockmans,I., Smets,N., Bouillon,R., Ellenberg,J. and Carmeliet,G. (2003) NuSAP, a novel microtubule-associated protein involved in mitotic spindle organization. *J. Cell Biol.*, **162**, 1017–1029.
80. Roostalu,J., Cade,N.I. and Surrey,T. (2015) Complementary activities of TPX2 and chTOG constitute an efficient importin-regulated microtubule nucleation module. *Nat. Cell Biol.*, **17**, 1422–1434.
81. Yokoyama,H. (2016) Chromatin-binding proteins moonlight as mitotic microtubule regulators. *Trends Cell Biol.*, **26**, 161–164.
82. Rieder,C.L. and Cole,R. (2000) Microtubule disassembly delays the G2-M transition in vertebrates. *Curr. Biol.*, **10**, 1067–1070.
83. Chang,C.H., Yu,F.Y., Wu,T.S., Wang,L.T. and Liu,B.H. (2011) Mycotoxin citrinin induced cell cycle G2/M arrest and numerical chromosomal aberration associated with disruption of microtubule formation in human cells. *Toxicol. Sci.*, **119**, 84–92.
84. Wittmann,T., Hyman,A. and Desai,A. (2001) The spindle: a dynamic assembly of microtubules and motors. *Nat. Cell Biol.*, **3**, E28–E34.
85. Bakhoum,S.F., Silkworth,W.T., Nardi,I.K., Nicholson,J.M., Compton,D.A. and Cimini,D. (2014) The mitotic origin of chromosomal instability. *Curr. Biol.*, **24**, R148–R149.

86. De,S., Tsimounis,A., Chen,X. and Rotenberg,S.A. (2014) Phosphorylation of alpha -tubulin by protein kinase C stimulates microtubule dynamics in human breast cells. *Cytoskeleton*, **71**, 257–272.

87. Kozielski,F., Riaz,T., DeBonis,S., Koehler,C.J., Kroening,M., Panse,I., Strozynski,M., Donaldson,I.M. and Thiede,B. (2011) Proteome analysis of microtubule-associated proteins and their interacting partners from mammalian brain. *Amino Acids*, **41**, 363–385.

88. Galigniana,M.D., Harrell,J.M., O'Hagen,H.M., Ljungman,M. and Pratt,W.B. (2004) Hsp90-binding immunophilins link p53 to dynein during p53 transport to the nucleus. *J. Biol. Chem.*, **279**, 22483–22489.

89. Uhlen,M., Fagerberg,L., Hallstrom,B.M., Lindskog,C., Oksvold,P., Mardinoglu,A., Sivertsson,A., Kampf,C., Sjostedt,E., Asplund,A. *et al.* (2015) Tissue-based map of the human proteome. *Science (80-.).*, **347**, 1260419–1260419.

90. Chambraud,B., Sardin,E., Giustiniani,J., Dounane,O., Schumacher,M., Goedert,M. and Baulieu,E.-E. (2010) A role for FKBP52 in tau protein function. *Proc. Natl. Acad. Sci. U.S.A.*, **107**, 2658–2663.

91. Kamah,A., Cantrelle,F.X., Huvent,I., Giustiniani,J., Guillemeau,K., Byrne,C., Jacquot,Y., Landrieu,I., Baulieu,E.E., Smet,C. *et al.* (2016) Isomerization and oligomerization of truncated and mutated tau forms by FKBP52 are independent processes. *J. Mol. Biol.*, **428**, 1080–1090.

92. Giustiniani,J., Chambraud,B., Sardin,E., Dounane,O., Guillemeau,K., Nakatani,H., Paquet,D., Kamah,A., Landrieu,I., Lippens,G. *et al.* (2014) Immunophilin FKBP52 induces Tau-P301L filamentous assembly in vitro and modulates its activity in a model of tauopathy. *Proc. Natl. Acad. Sci. U.S.A.*, **111**, 4584–4589.

93. Giustiniani,J., Guillemeau,K., Dounane,O., Sardin,E., Huvent,I., Schmitt,A., Hamdane,M., Buée,L., Landrieu,I., Lippens,G. *et al.* (2015) The FK506-binding protein FKBP52 in vitro induces aggregation of truncated tau forms with prion-like behavior. *FASEB J.*, **29**, 3171–3181.

94. Gunawardana,C.G., Mehrabian,M., Wang,X., Mueller,I., Lubambo,I.B., Jonkman,J.E.N., Wang,H. and Schmitt-Ulms,G. (2015) The human tau interactome: binding to the ribonucleoproteome, and impaired binding of the proline-to-leucine mutant at position 301 (P301L) to chaperones and the proteasome. *Mol. Cell. Proteomics*, **14**, 3000–3014.

95. Castello,A., Fischer,B., Frese,C.K., Horos,R., Alleaume,A.M., Foehr,S., Curk,T., Krijgsveld,J. and Hentze,M.W. (2016) Comprehensive Identification of RNA-Binding Domains in Human Cells. *Mol. Cell*, **63**, 696–710.

96. Park,S., Osmers,U., Raman,G., Schwantes,R.H., Diaz,M.O. and Bushweller,J.H. (2010) The PHD3 domain of MLL Acts as a CYP33-regulated switch between MLL-mediated activation and repression. *Biochemistry*, **49**, 6576–6586.

97. Gustafson,C.L., Parsley,N.C., Asimgil,H., Lee,H.-W., Ahlbach,C., Michael,A.K., Xu,H., Williams,O.L., Davis,T.L., Liu,A.C. *et al.* (2017) A slow conformational switch in the BMAL1 transactivation domain modulates circadian rhythms. *Mol. Cell*, **66**, 447–457.

98. Arévalo-Rodríguez,M., Pan,X., Boeke,J.D. and Heitman,J. (2004) FKBP12 controls aspartate pathway flux in Saccharomyces cerevisiae to prevent toxic intermediate accumulation. *Eukaryot. Cell*, **3**, 1287–1296.

99. Riggs,D.L., Cox,M.B., Tardif,H.L., Hessling,M., Buchner,J. and Smith,D.F. (2007) Noncatalytic role of the FKBP52 peptidyl-prolyl isomerase domain in the regulation of steroid hormone signaling. *Mol. Cell. Biol.*, **27**, 8658–8669.

100. Monneau,Y.R., Soufari,H., Nelson,C.J. and Mackereth,C.D. (2013) Structure and activity of the peptidyl-prolyl isomerase domain from the histone chaperone Fpr4 toward histone H3 proline isomerization. *J. Biol. Chem.*, **288**, 25826–25837.

101. Leung,A., Jardim,F.-P., Savic,N., Monneau,Y.R., González-Romero,R., Gudavicius,G., Eirin-Lopez,J.M., Bartke,T., Mackereth,C.D., Ausió,J. *et al.* (2017) Basic surface features of nuclear FKBPs facilitate chromatin binding. *Sci. Rep.*, **7**, 3795.

102. Blair,L.J., Baker,J.D., Sabbagh,J.J. and Dickey,C.A. (2015) The emerging role of peptidyl-prolyl isomerase chaperones in tau oligomerization, amyloid processing, and Alzheimer's disease. *J. Neurochem.*, **133**, 1–13.

103. Cao,W. and Konsolaki,M. (2011) FKBP immunophilins and Alzheimer's disease: a chaperoned affair. *J. Biosci.*, **36**, 493–498.